Seismic noise cross-correlation in the urban area of Benevento city (Southern Italy)

Maurizio Vassallo[1], Raffaella De Matteis[2], Antonella Bobbio[3], Giuseppe Di Giulio[1], Guido Maria Adinolfi[4], Luciana Cantore[1*], Rocco Cogliano[5], Antonio Fodarella[5], Rosalba Maresca[2], Stefania Pucillo[5], Gaetano Riccio[5]

[1] Istituto Nazionale di Geofisica e Vulcanologia, Viale Francesco Crispi 43/47, 67100, L' Aquila, Italy.
[2] Dipartimento di Scienze e Tecnologie, Università degli Studi del Sannio, Via dei Mulini, 82100 Benevento, Italy
[3] Istituto Nazionale di Geofisica e Vulcanologia - Osservatorio Vesuviano, Via Diocleziano, 328, 80145 Napoli, Italy
[4] Dipartimento di Fisica, Università degli Studi di Napoli Federico II, Complesso Universitario di Monte S.Angelo, Via Cinthia, 80124 Napoli, Italy
[5] Istituto Nazionale di Geofisica e Vulcanologia, c.da Ciavolone, Grottaminarda 83035, Avellino, Italy.
[*] Now at Ministero dell'Istruzione dell'Università e della Ricerca.

Corresponding author
Maurizio Vassallo
Istituto Nazionale di Geofisica e Vulcanologia, Viale Francesco Crispi 43/47, 67100, L' Aquila, Italy
email: maurizio.vassallo@ingv.it
+39 0862709120

Abstract
In the last decade the use of passive methods has become appealing in reconstructing the properties of the propagation medium by seismic ambient noise data, without the use of localized natural or artificial sources. A temporary seismic network was installed in the urban area of Benevento (southern Italy) in order to characterize the shallow structure of the city using stable methods for the analysis of the seismic noise continuously acquired by stations. The city of Benevento is one of the italian areas with highest seismic hazard, and at present the region is affected by low energy swarms and sparse events (Ml<=4.1). It has been struck by several destructive historical earthquakes, the strongest of which occurred in 1456, 1688, 1805 with associated MCS intensity up to X–XI. We used the sixteen seismic stations installed in Benevento to record ambient noise for about 1 month. The stations were equipped with different seismic instruments: i) digitizers Quanterra Q330 connected to Le3d-5s short-period sensors; ii) Nanometrics Centaur digitizers coupled with Trillium Compact 120s broad-band velocimeters; iii) one station with Episensor force balance accelerometer connected to a D6BB-DIN Staneo digitizer. Inter-stations Green's functions were reconstructed by the cross-correlation of continuous ambient noise data, and surface waves signals were extracted from Green's Functions (GFs) for investigating the elastic properties of the subsurface structure. In this regard, we performed the beamforming analysis to test the hypothesis of isotropy distribution of noise sources on which the cross-correlation method is based, and the particle motion analysis to confirm the presence of surface Rayleigh waves in the GFs. We analyzed the temporal stability of the cross- correlated signals and the results show that two weeks of continuous measurements are sufficient to stabilize the surface waves signal extracted from the GFs. The phase velocity dispersion curves are computed for 115 station pairs through the use of a far-field representation of the surface-wave GFs and an image transformation technique. Our strategy based on cross-correlation analysis provides robust phase-velocity dispersion curves that vary approximately from 1.4 km/s at 0.7 Hz to 0.6 km/s at 5 Hz. Different pairs were selected for the inversion of phase-velocity dispersion curves aimed to derive 1D shear-wave velocity (Vs) profiles (up to a maximum depth of about 500 m) representative of some areas of the city characterized by different soil deposits.

Keywords: seismic noise; seismic interferometry; surface waves and free oscillations.

1. Introduction

The city of Benevento is located in the Sannio region (southern Italy), one of the italian areas with highest seismic hazard. It has been struck by several destructive historical earthquakes and at present the region is affected by low energy swarms and sparse events (Ml<=4.1; Milano et al., 2006, Adinolfi et al., 2015). For its high seismic potential and historical heritage, this area has been the subject of several studies focused on the shallow geological structure and local site effects (Iannaccone et al., 1995; Pescatore et al., 1996; Maresca et al., 2003, Senatore et al., 2019). The results of these studies suggest that Benevento area is characterized by heterogeneous lithologies and widespread soft soil conditions responsible of seismic response variation over short distances in the urban area (Maresca et al., 2003; Improta et al., 2005; Di Giulio et al., 2008). These studies are usually planned in the context of seismic microzonation which is used to assess the soil class required by the current Italian building code (Norme Tecniche per le Costruzioni 2008, NTC08) and for territorial planning of the Municipality.
The shear-wave velocity (Vs) of subsoil is a key parameter for studies of seismic microzonation. In urban areas, Vs profiles are mainly retrieved by non-invasive geophysical methods based on active sources, such as multichannel analysis of surface waves (MASW, Park et al., 1999) and shallow tomography, and passive sources such as array analysis (SPAC spatial autocorrelation, Aki, 1957) and refraction microtremor (REMI, Louie, 2001). Shear-wave velocity can be also directly measured from invasive in-situ tests that, however, provide only punctual information and they become very expensive or unusable to characterize the properties of deeper soil layers. The

knowledge of a 3D shear-wave velocity model can be an useful tool but, in urbanized area, such as Benevento, the tomographic techniques based on natural or artificial sources are generally not viable, both for the low seismic activity, and for authorized limited energy of the active sources. In such cases, the continuously recorded seismic ambient noise may represent a cheap alternative tool to investigate the elastic properties of the propagation medium and for the reconstruction of a 3D velocity model of subsoil.

In the last ten years, the studies based on cross-correlations between pairs of receivers are becoming popular to provide detailed velocity models. It has been theoretically shown that the cross-correlation of ambient noise recorded at pairs of stations can provide an estimate of the Green's function between the receivers (Larose et al., 2004; Sanchez-Sesma & Campillo, 2006). This has been proven by several applications in different areas of the world and in different geological environments, both at regional and local scales (Shapiro et al., 2005; Roux, 2009; Duputel et al., 2009; Picozzi et al., 2009; Li et al., 2010; Pilz et al., 2013; Vassallo et al., 2016). Cross-correlation analyses in urban environment are still few (Nunziata et al., 2009) but in recent years they have experienced a rapid increase (Shirzad & Shomali, 2015; Obermann et al., 2015; Lehujeur et al., 2015; Pastén et al., 2016; Asano et al., 2017). In such context, the manmade activities represent the main sources of passive seismic energy, especially in the high-frequency range (approximately > 1 Hz). Further, a basic assumption of the cross-correlation analysis is the equipartition of energy, which can fails in presence of directional sources of noise.

The goal of this study is to develop and test stable methods based on seismic noise cross-correlation to characterize the shallow structure of Benevento, a city in southern Italy affected by high seismic hazard, at a spatial scale never investigated before now (~0.5 km). We apply the cross-correlation technique to ambient noise recorded in the urban area in order to retrieve the S-wave velocity profiles at depth greater than usually explored for microzonation studies (usually a few tens of meters). Moreover the spatial distribution of the seismic network, through the cross-correlation analysis at all pairs of stations, allows to obtain average information on the spatial variation of the S-wave velocity unlike the Vs profiles obtained in the microzonation studies that are punctual or related to a very limited areas. A detailed knowledge of the velocity model is a basic tool in the seismic hazard analysis for the simulation of more physically realistic ground motion time histories. In fact, in the framework of hazard studies the most advanced approaches estimate ground motion parameters not using the empirical attenuation relationships, but calculating the synthetic seismograms starting from the knowledge of the earthquake source parameters and the properties of the propagation medium.

We installed for one month a seismic network consisting of 16 stations deployed over an area of about (3x4) km^2 in the city and its surroundings (Figure 1a). In this paper, we describe the seismic network and its components; then, we characterize the properties of ambient noise through seismic analyses applied to single station and to the whole array (Power Spectral Density, H/V spectral ratios, beamforming, f-k analysis). These analyses will be used to check the hypothesis of applicability of the cross-correlation method on noise data acquired in urban area. After presenting the seismic network and noise properties, we compute the cross-correlation of continuous ambient noise for all stations pairs, for different components and varying the frequency content. We then isolate the surface-wave contribution from which we retrieve the dispersion curves in term of phase velocity. Finally, from the inversion of selected dispersion curves, we obtain 1D velocity profiles for several areas of the city.

2. Geological Setting

Benevento is located in an inner sector of the southern Apennine chain, at the confluence of Calore and Sabato rivers. The geology of the city and of its surrounding areas is deeply influenced at large scale by the Neogene Southern Apennines kinematic evolution (Improta et al. 2010), and at small scale by the Quaternary activity of the Calore and Sabato rivers. From Upper Pliocene to the present, NW-SE striking normal faults related to a prevailing NE-SW extension, and NE-SW

striking faults affected this inner sector of the southern Apennines. Strong seismic events occurred in the past (1456, 1688, 1702, 1805) mainly along the NW-SE normal fault system, with associated MCS intensity (Is) up to X–XI (Rovida et al., 2011). A moderate magnitude 6.1 earthquake occurred in 1962, and recently, smaller seismic sequences lasted several months occurred (1986, 1990, 1997, 2012) (Vilardo et al., 2003; Milano et al., 2004, Adinolfi et al., 2015). Peak ground acceleration with 10 percent of being exceeded in 50 years is estimated for the studied area up to 0.275 *g* (Meletti & Montaldo, 2007).

Benevento lies in a Plio-Pleistocene tectonic basin filled by marine and continental deposits. The geological map of the study area is shown in Figure 1b. Most of the pre-quaternary substratum is formed by marine sediments of the Ariano Unit (Middle Pliocene; Peg, Ps, and Pag in Fig. 1b). These deposits, forming a simple monocline structure dipping toward N-NE, overlie the flysch deposits of the Meso-Cenozoic Lagonegro Basin. Geophysical data show that the Pliocenic substratum reaches its maximum thickness (250 m) in correspondence of the Sabato river valley (Pescatore et al., 1995). The oldest terrains belonging to the Lagonegro Unit (Miocene, M in Fig. 1) crop out NE of Benevento, where form the Capodimonte hill. They are formed by stiff and deeply deformed marl and shale with layers of sandstone. The deposits of the Ariano Unit (Peg, Ps, and Pag in Fig. 1b) include terrigenous successions formed by clay, sand and sandstones interspersed with conglomeratic layers. These deposits mostly crop out at SW of Benevento, forming the Gran Potenza ridge. Formed into a middle Pliocenic piggy-back basins, the Gran Potenza Ridge synorogenic deposits have not been highly deformed during the tectonic evolution. In the Sabato river valley, the top of the pre-quaternary substratum lies at an elevation of about 120 m a.s.l. and progressively dips to 80 m a.s.l. towards the confluence with the Calore river, due to tectonic displacements (Iannaccone et al., 1995). Quaternary continental deposits were deposited in depressed areas delimited by tectonic lineaments with E-W trends, as in the Calore valley. The Quaternary sediments, which often reach a thickness of several tens of meters, show marked differences in their lithological and mechanical properties. We can distinguish three different lithotypes:

1) Middle Pleistocene (Riss) conglomerates (AA_{AB} in Fig. 1b); this deposit crops out along the Calore river, and forms the Benevento hill. The old town of Benevento is situated on the NW portion of the hill. These are very stiff cemented conglomerates, with sandy lenses, up to 100 m thick, including also layers of dense gravels and silty-sands. These deposits acted as high impedance rocks, when the seismic site amplification was estimate at surface (Iannaccone et al., 1995; Improta et al., 2005).

2) Late Pleistocene terraced alluvia (Al_{2B} in Fig. 1b), which are dominant in the Calore river. They are composed by dense and sometimes cemented gravels, with silty to sandy lenses.

3) Fluvio-lacustrine succession of the Sabato river (Al1 in Fig. 1b), composed of thinly stratified clay with sandy layers with organic content. This formation does not exceed 40 m in thickness.

Generally, debris, colluvial soils, and pyroclastites cover all the formations described above. A range of velocity values for the main geological units of Benevento was mainly found by the results obtained from cross-hole and down-holes surveys (Di Giulio et al., 2008). Several studies were carried out by different authors on the seismic site response of Benevento (Iannaccone et al., 1995; Maresca et al., 2003; Improta et al., 2005). The most recent and detailed survey proposed by Di Giulio et al. (2008) combined seismological and geological data to providing a seismic classification of the area. These authors distinguished three different zones in Benevento with different levels of soil amplification (Di Giulio et al., 2008): level I with no significant site effect (AA_{AB} in Fig. 1b), level II with 1D high frequency (>4 Hz) resonance effects (Al_1 in Fig. 1b), and level III with moderate broad-band (1-10 Hz) amplification (Peg, Ps, Pag, and Al_{2B} in Fig. 1b).

3. Setup of experiment

Starting from 2nd May 2016, an experiment was carried out in Benevento urban area installing 16 temporary seismic stations to record ambient noise. Most of stations (11) are equipped with three-

components short-period seismometer (Lennartz - LE-3D/5s) and Quanterra acquisition system (Kinemetrics Q330); four stations are equipped with broad-band seismometer (Nanometrics – Trillium compact 120s) and Centaur digital recorder (Nanometrics). Only one station (BENI), permanently installed inside a building of Sannio University has a three-axial force balance accelerometer (Kinemetrics - Episensor FBA ES-T) and a digitizer designed for permanent seismic station (Staneo - D6BB-DIN). All acquisition systems consist of a high resolution 24-bit ADC and a precision GPS clock. The technical features of each station are shown in Table 1 and the working period of each station is detailed in Figure S1.
The raw data were acquired in mseed format and then converted in 24 hours long SAC files, collecting about 1500 (three components) waveforms. During the acquisition period a low magnitude seismic sequence occurred at ~ 10 km E of Benevento. The sequence started on 17th May 2016 with the main shock at 08:45:31 UTC with M_L 2.6. During the sequence about 30 events were recorded with magnitude between 1.0 and 2.4. The events were recorded by the temporary seismic network and an example of the waveforms is shown in Figure 2. The variability of amplitudes and frequency content of traces recorded by different stations is indicative of the different local site effects of the investigated area.

4. Preliminary noise analysis

4.1 Power Spectral Densities (PSD) and spectrograms

In order to characterize the seismic background noise at the seismic stations of the temporary Benevento network, we computed the Power Spectral Density (PSD) using the continuous three-components data acquired in 30 days by 16 sensors. All the analysis was performed by PQLX (PASSCAL Quick Look eXtended), an open-source software build for evaluating seismic station performance and data quality. PQLX server calculates Power Spectral Densities (PSD), and Probability Density Functions (PDF) from the waveform data and the corresponding response files, then for a quick access to the results, it stores them to a MySQL database. The computation of PSD and PDF is based on the algorithm by McNamara & Buland (2004). Following this algorithm, the PSD were obtained on mobile windows of signal of one hour with 50% overlap. For each seismic channel, the software calculates the PDF by the distribution of the PSD values at each spectral interval. PDFs provide the occurrence probability of a fixed seismic signal level in a fixed frequency interval.
Figure 3 shows the PDFs and relative spectrograms computed from the vertical component of continuous seismic noise recorded by four stations of Benevento network. As quantitative estimation of noise levels, we also computed the 10th and 90th percentile and modal curve which are drawn in Figure 3 with dotted lines and black line, respectively. Even being in a highly urbanized area, the PDFs are within the curves computed by Peterson (1993), which represent the high and low noise model. The cultural noise dominates the frequency spectrum at short periods (approximately < 1s); in this range the spectrograms clearly show the diurnal and workweek variations (Fig. 3). We used the PSDs also as a tool to check the proper functioning and the health status of the seismic stations during all the acquisition period.

4.2 H/V spectral ratio

The horizontal-to-vertical (H/V) noise spectral ratio (Molnar et al., 2018) was computed at each station of the temporary Benevento network (Fig. 4). The seismic signals were processed using the *geopsy* tool (www.geopsy.org) that employs an antitrigger algorithm to remove spikes and short transients occurring in the records. The continuous recording mode allowed to select 24 hours for the H/V analysis. We repeated the analysis during different days and using daily and nightly hours; we observed differences on the spectra of the three components of the ground motion but the final H/V spectral ratio does not change substantially. For the H/V analysis we used a running time-window of 60 s, and in each window we removed the mean, the linear trend and applied a 5% cosine taper. Then, we calculated the Fourier amplitude spectra smoothed following the Konno &

Omachi (1998) filter using a coefficient of 40 for the bandwidth. The two horizontal spectra were combined by a quadratic mean, and then divided by the vertical spectrum to get the H/V ratios. Finally, the mean H/V ratio and the standard deviation were computed by a geometrical average of the H/V ratios from all the selected windows.
The results show different shapes of the H/V curves within the Benevento area, confirming the large variability of resonance frequencies as shown by past studies focused on noise ratios (Improta et al., 2005). The lowest frequency peaks are observed around 0.8 Hz in the northern part of the city (SPSA and NEW1 stations) suggesting the presence of a deep seismic contrast (> 100 m) in the subsurface velocity structure. A low-frequency peak at 1 Hz is shown at three stations (SMA1, SMA2 and DEFI); this 1 Hz peak is followed in the H/V curve by a trough indicating a possible connection with the ellipticity of Rayleigh waves. The 1 Hz peak is probably present to other sites (e.g. ARC1, GIAN, CRE2 and SACG) but is very weak in the amplitude level (< 2) and therefore the assignment of the fundamental resonance at these sites is dubitative.
Resonances in the intermediate frequency-band (2-5 Hz) are also observed (RUMO, BENI, SACG, CRE2, GIAN, PAX1 and PAPI) probably due to a velocity contrast occurring at relatively shallow depth (< 50 m). Not clear H/V peaks are shown by SAB1 situated in the alluvial deposits of Sabato river, with the H/V indicating a bump-like shape at 1-2 Hz followed by a strong decay of amplitudes in the high-frequency range. Secondary peaks at about 10 Hz are also present at different sites (CAL1, COST, NEW1 and GIAN) and could be ascribed to thin layers of cover or debris soils.

4.3 Beamforming

The extraction of Green's function from noise cross-correlation is based on the hypothesis of isotropic distribution of noise sources. To test this hypothesis we performed a beamforming analysis based on fk (frequency-wavenumber) method which assumes propagation of horizontal plane waves across the array. In the beamforming analysis, the sum of coherent signal from single stations is used to increase the signal-to-noise ratio (SNR) and the time shifts of the signal between the array stations estimate the seismic apparent velocity and back azimuth of the signal crossing the array. We applied the beamforming to different days of data acquired by the array stations and filtered in the 0.5-0.9 Hz and 0.9-2.0 Hz frequency bands where we expected the main signal from the cross-correlation at the experiment scale. The data were discretized in time-windows and for each one, the relative power, the back-azimuth and the slowness of the signal were computed. Examples of beamforming results obtained for the day 2016-05-09 are shown in Figure 5. Relative power, backazimuth and slowness are represented both as a function of time and in a polar plot which sums the relative power in gridded bins. In the case of filtered signal between 0.9 and 2.0 Hz, the power level is comparable in all the windows and there isn't a predominant direction of signal. In the frequency between 0.5 and 0.9 Hz, instead, the characteristics of the signal sources are time dependent. Between the 00 and 05 UTC hours and after the 22 UTC hour, there is a coherent signal that propagates across the array with slowness of about 0.3-0.5 s/km and backazimuth in the range 170°-200°. Between the 05 and 22 UTC hours. the noise is isotropic and propagates with slowness higher than those observed during the night hours.

5. Cross-correlation analysis

For cross-correlation analysis, we used the method proposed by Bensen et al. (2007), and schematised in the block diagram shown in Figure S2. We corrected the three-components of continuous velocity traces for instrumental response, after a removal of the mean and the linear trend. The data were band-pass filtered between 0.4 Hz and 10 Hz. In this frequency band the response of the different seismic sensors used in the experiment is flat (Figure S6); this assures us that the seismic noise has been properly recorded at each station irrespective of instrumentation installed. The data processing was different for the station equipped with accelerometer. In this case, after the correction for instrumental response, the 24 hours long data were resampled at 100 Hz using the Wiggins (1976) weighted average-slopes interpolation method, a symmetric Hanning taper was applied to each end of data, then we integrated the resulting traces to derive velocity time-

series and we applied band-pass filtered between 0.4 Hz and 10 Hz. At this point, the obtained velocimetric traces have been processed as those related to velocimetric sensors for the computation of cross-correlation.
Each continuous trace was cut in windows of 24 hours length, starting from the midnight of each day. The beamforming results suggest that in a such windows length, the most part of the signal does not have a predominant direction and can be assumed as isotropic. This is especially true in 0.9-2.0 Hz frequency band where, as described below, most of the phase velocity values are estimated from the cross correlation analysis.
In order to equalize the amplitude of the signal we applied the one-bit normalization, which retains only the sign of the trace. In this way, we reduced the effect of artefacts related to anomalous amplitudes (earthquakes, instrumental irregularities and very energetic arrivals) on the cross-correlated signals. Then, we applied a spectral whitening to the traces in order to equalize their spectral amplitude content. This equalization is adopted to minimize the contribution of both most energetic signals present in the data spectra and possible persistent monochromatic sources. Finally, the available synchronized traces were cross-correlated at each pair of stations. The cross-correlations were calculated from 120 pairs of stations and for the different components (vertical, radial and transversal, the last two computed using the line joining the stations pairs) for a total number of 10800 cross-correlation (CC) functions. For each pair of stations, the daily cross-correlations were added to each other for the entire period of the experiment, providing a stacked cross-correlation function. The stack was computed from time to time by adding a new daily cross correlation function, verifying that the CC stack becomes stable using 12 days of data.
The stacks for three components (ZZ, ZR, ZT) of the cross-correlation tensor, organized for increasing inter-station distance, are shown in Figure 6 for two different frequency bands (0.5-1.0 Hz and 1.0-2.0 Hz). The cross-correlation signals are two-sided time functions with the positive time coordinates corresponding to waves propagating from the northernmost to southernmost station for each pair. From the Figure 6 is clear that energetic seismic phases are symmetric with respect to zero time with amplitude slightly varying between the causal and acausal parts. Furthermore, Figure 6 shows that the most energetic seismic phase follows a linear trend corresponding to a surface wave velocity compatible with the expected velocities of the investigated area (Di Giulio et al., 2008; Senatore et al. 2018). Theoretical arrival times of a surface wave with velocity of 2000 m/s, 1500 m/s, 1000 m/s and 500 m/s are also superimposed on the sections shown in Figure 6. The main signals are clear in both the frequency ranges (0.5-1.0 Hz and 1.0-2.0 Hz) in the ZZ and ZR components of cross-correlation. In the ZT component, instead, this phase has a very low signal-to- noise ratio and is barely recognizable in the cross-correlation seismic section.
To compute the velocity of the phase emerging in the cross-correlation sections (Fig. 6), we applied a velocity analysis to the ZZ cross-correlation functions. The used method is similar to CVS (Constant Velocity Stack, Yilmaz, 1987) velocity analysis, very popular in active seismic processing. The cross-correlation functions were filtered in different frequency band starting from 0.5 Hz up to 2.5 Hz. For each filter the cross-correlation functions were shifted back in time according to the theoretical surface traveltimes calculated for different constant velocities starting from 400 m/s until 2500 m/s using a sample rate of 100 m/s. For each velocity correction we computed the stack function for shifted cross-correlations that is used to estimate the presence of a horizontally aligned phase in the seismic section. For each filter, the velocity associated to the maximum of stack estimates the phase velocity at the considered frequency. The values of maximum (between 0 and 120) provide a guidance on the goodness of the estimates, a velocity value is associated to a frequency only when the maximum of stack is higher than 10. The results of analysis (Fig. 7) show a clear decrease of velocity with the frequency, typical trend of the surface waves. The estimated velocities are between 1500 m/s (at 0.5 Hz) and 700 m/s (at 2.0 Hz). At frequencies higher than 2.0 Hz the maximum of the stack function is lower than 10 indicating a degradation of the S/N ratio of signal, or that a simple velocity correction is no longer appropriate to align the seismic phase at these frequencies.

In order to study the stability with time of the most energetic signal obtained by cross-correlation, we represented all the CCs computed for the whole duration of experiment. Figure 8 shows examples of cross-correlations filtered in the 1.0-2.0 Hz frequency band, computed for six pairs of stations (PAX-ARC1, GIAN-DEFI, CRE2-COST, CRE2-BENI, DEFI-COST, PAPI-COST) using the entire dataset. For each pair, the horizontal axis represents the time lag of the cross-correlation function whilst the vertical axis corresponds to the time in Julian days at which the ambient noise was recorded. The color scale is proportional to the amplitude of the cross-correlation function where each trace is normalized to its maximum value. The corresponding stack functions are shown at the top of each panel. For all the six pairs, selected at different interstation distances, we observe a good coherence in both the causal and acausal phases over the whole duration of experiment. In same cases we observe that the cross-correlation functions are asymmetric around zero. Specifically, the pairs CRE2-BENI, CRE2-COST and DEFI-COST show larger amplitudes in the acausal signals. Nevertheless, the presence of clear causal and acausal signals, albeit with different amplitudes, evidences a wider azimuthal distribution of the noise sources, as confirmed by the beamforming results. Figure 8 shows both that the arrival time of the most energetic seismic phase increases with the inter-station distance, and it depends on azimuth of the line joining the pair. This azimuthal dependence is evident in Figure 8 for the two pairs of stations CRE2-COST and CRE2-BENI, which have the same inter-station distance but different azimuth.

Whereas also seasonal trends in the wavefield can affect the computed cross-correlations, we analyzed the few stations of Benevento network having 16-months of continuous data. For these stations, the seasonal variations and CC stability vs time were analyzed in a time window longer than window used for our experiment. The pair CRE2-CAL1 has about 16-months of continuous seismic data starting from 10th April 2015. Therefore, the cross-correlation for this stations pair has been computed over the entire period in the frequency range 0.8-4 Hz. The results are summarized in the Figure 9 that shows a clear stability of CCs over time, and the stack computed on 16-months is very similar to that calculated over one month (the correlation coefficient between the two waveforms of 0.93).

The dominant signal in the cross-correlations between 0.5 and 2 Hz propagates with velocity compatible with the velocities of the surface waves in the investigated area. Furthermore, this phase is present mainly on the ZZ and ZR components of the cross-correlation tensor, suggesting that it is a surface wave. To further test that the energy, which emerges on the CC functions, does in fact consist of surface waves, we performed the particle motion (PM) analysis on the most energetic signal retrieved in the seismic sections of Figure 6. The analysis was carried out on three different pairs of stations (GIAN-COST, DEFI-COST and PAPI-COST) having different interstation distances. The vertical-vertical (ZZ), the vertical-radial (ZR) and vertical-transverse (ZT) components of CC tensor were selected for the PM analysis on both the causal and acausal parts of the most energetic signal. The results for the three different pairs are shown in Figure 10. The PM was calculated on a time window (pink and blue windows for acausal and causal signals, respectively) containing the prominent energy of the CC functions. In all cases, the PM shows larger amplitudes mainly confined on ZZ and ZR components whilst the ZT components show the lowest amplitudes. In both causal and acausal signals and for all the stations pairs, we observe a retrograde elliptical motion in the vertical-radial and vertical-transverse plains; this is compatible with the expected PM of Rayleigh surface waves.

6. Dispersion curves and 1D velocity models

Both phase and group velocities are useful expressions of properties of the propagation media that can be extracted from cross-correlation signals to pairs of stations. In our case we used an ad hoc spectral analysis (based on a far-field representation of the surface-wave GFs and an image transformation technique) for the determination of phase velocities dispersions from cross-correlated data. We found that the proposed ad hoc method allowed us a simpler identification of the phase velocities with respect to the determination of the group velocities carried out with

standard frequency-time analysis technique (FTAN, Levshin et al., 1972). In our case, the simplest identification of phase velocities turned into a more reliable and accurate phase measurements compared to the group velocity measurements. This was also highlighted by other authors who found advantages in working with phase velocities (Boschi et al., 2013) and that retrieved uncertainty of phase measurement of waveforms much smaller than that those of group velocity measurement based on the peak of waveform envelope (Bensen et al., 2007, Luo et al., 2015).
The proposed spectral analysis extracts the phase velocity dispersion curves from the CC functions computed using different station pairs. First, we band-pass filtered the cross-correlations at central periods from 0.2 s to 2 s, with a step of 0.005 s. In the case of symmetric CC function the filter is applied on symmetric component of CC (the stack of the positive and reversed negative time of CC). For non-symmetric CCs, the analysis was performed on the side with the larger amplitude. A surface velocity range from 200 m/s to 2500 m/s was used to define the part of traces with useful signal for the analysis. For each pair of stations, the amplitudes of retrieved traces were organized in a matrix where each column represents an amplitude normalized of cross-correlation function filtered at a certain period T (t-T image). This matrix was used to construct the phase velocity-period ($c-T$) image based on the transformation technique proposed by Yao et al. (2006). Three examples of phase velocity-period images obtained for different pair of stations are shown in Figure 11. In each phase velocity-period image, there are multiple phase velocity dispersion branches. CVS analysis (described in the paragraph *Analysis of cross-correlations*) is able to indicate the correct branch to follow for the picking of dispersion curve. The CVS analysis provides velocity of 1000 m/s at 1 Hz (black dots in Figure 11). Moreover, since the analysis was made on surface waves, we expect an increase of the phase velocity with increasing period. Bearing in mind these considerations, the dispersion curve (white line) was identified following the branch closest to the velocity values obtained from the CVS analysis and that shows an increase of the phase velocity with period. The dispersion curve was picked in period ranges defined differently for the various station pairs. The picks were determined only for period for which the distance between the stations is longer than one wavelength. The selected branch shows a discontinuous pattern with the decrease of the period. The minimum period for picking was defined when the pattern assumes a discontinuous character. The illustrated technique is applied to 115 station pairs. In order to validate the proposed spectral analysis method, we used also an alternative method based on phase velocity estimated directly from the zero crossing of the real part of correlation spectrum (Aki, 1957). We used GSpecDisp tool (Sadeghisorkhani et al., 2018), a matlab GUI package that provides an interactive environment for the phase velocity based on the spectral-dispersion method in the frequency domain, using time-domain correlations as input. Generally, the two methods give very similar (almost overlapping) dispersions curves (Figure S3). Some differences are observed on a few cases and are mainly observed between 3.5 and 5 Hz, with differences between the two curves at maximum of 10% in terms of the estimated velocity values.
Figure 12a shows the 115 dispersion curves obtained with the proposed spectral method. They are defined in the 0.7-5 Hz frequency range with values between 400 m/s and 1500 m/s. The mean curve computed using all dispersion curves (blue curve in Fig. 11a) shows a decreasing trend with increasing frequency with velocity of 1050 m/s at 0.95 Hz and 700 m/s at 5 Hz. All the dispersion curves were used to define a Probability Function (PDF) of phase velocity in each investigated frequency (Fig. 11b). Between 0.7 Hz and 2 Hz, the PDF shows two peaks that reveal a bimodal character of velocity distribution at these frequencies. The first PDF peak have probability between 0.3 and 0.4, the second peak is observed at higher velocity values respect the first one and is characterized by probability values between 0.10 and 0.12. The peak associated to the maximum of PDF shows a decreasing trend with the frequency and it is observed at about 1150 m/s at 0.7 Hz, and it reaches values of about 750 m/s at 2 Hz. Between 2 Hz and 5 Hz, the PDF has only one maximum with lower values than those observed in the previous frequency range. This characteristic is a linked index of a greater dispersion of the velocities observed at these frequencies.

As a further validation of the proposed ad hoc method, we compared the averaged dispersion curve with the results obtained from a conventional f-k analysis. The daily raw data recorded by the Benevento network were analysed through a conventional f-k (frequency-wavenumber) beamforming (Lacoss et al., 1969; Horike, 1985). The 16 stations of the network were considered as a 2D seismic array, with a minimum and maximum interdistance among stations of about 390 and 3800 m, respectively. We computed the alias and resolution theoretical limits from the array response functions, and then we measured a dispersion curve within these limits using the geopsy tool (www.geopsy.org) considering the vertical component. Figure 12c shows clear dispersion properties of the daily seismic signals within the reliable frequency band (0.4-2 Hz). To evaluate the stability with time of the f-k results, we repeated the array analysis in time using three different days (Figure S4). The f-k results along the selected times are very consistent, showing apparent velocities spanning approximately from 1800 m/s to 700 m/s (at 0.4 and 2 Hz, respectively). For comparison, the average dispersion curve derived from cross-correlation analysis with error bars were overlaid to the f-k results (Fig. 11c). The agreement between the dispersions estimated from array analysis (f-k domain) and cross-correlation analysis validates the goodness of the two typologies of methods in capturing the surface-wave velocities from the seismic signals.

We used the phase velocity dispersion curves shown in Figure 12a to estimate representative shear-wave velocity (Vs) profiles for areas characterized by different shallow geological unit (filling man made ancient deposits; conglomerates and alluvial deposits). For each geological unit we selected the dispersion curves obtained from two station pairs:

i) BENI-ARC1 and GIAN-ARC1 for the filling man made ancient deposits (F-Cl in Fig. 1b);

ii)GIAN-CRE2 and SACG-GIAN for the conglomerates unit in Cretarossa hill (Peg in Fig. 1b);

iii) SAB1-RUMO and NEW1-COST for the alluvial deposits of Sabato and Calore rivers (Al2B in Fig. 1b), respectively. Furthermore, the SMA2-PAPI pair was also considered because in this case the observed dispersion curve shows clearly the presence of a velocity reversal in the profile (i.e. not normally dispersive sites). The selected dispersion curves were estimated in the frequency range 1-5 Hz. We inverted them as phase Rayleigh-wave to estimate a Vs profile for each pair of stations. For the inversion of the dispersion curves we used the *HV-inv* code (García-Jerez et al., 2016; Piña-Flores et al., 2017), based on the diffuse field assumption (García-Jerez et al., 2013) and theoretical connection between the elastodynamic Green's function (imaginary part) and H/V curve (Sanchez-Sesma et al., 2011; Molnar et al., 2018). Because the large variability of the H/V curves (Figure 4), we preferred to include in the inversion step only the dispersion curve, for this reason the *HV-inv* code worked in the assumption that dispersion is related only to Rayleigh waves without the contribution of the diffuse wavefield. The experimental dispersion curves (Fig. 12a), obtained at each pair of stations, were first logarithmically smoothed using 30 points. To taking into account an error in the estimates of the dispersion curves, we added to each curve (Figure 13) a 5% error proportional to the measured phase-velocities. As model parameterization we considered four layers (over half-space) where the free parameters (Vp, Vs, thickness and Poisson ratio) are allowed to vary within each layer during the inversion procedure. The density, which has a lower influence on the dispersion curve (Xia et al., 1999), was fixed to 2 kg/m^3. The thickness within each layer was free to vary between ⅓ of the minimum wavelength and 150 m. The first limit is associated to the maximum frequency of analysis and is usually assumed in surface-wave analysis as the minimum resolvable layer (Foti et al. 2018), whereas the maximum depth of investigation was experimentally linked to the half of the maximum wavelength. These limits connected to the minimum and maximum wavelengths are empirically adopted and valid as first order of approximation, because in principle the resolution and maximum resolved depth are connected to the velocity structure of the target site (Renalier et al., 2010). For sake of simplicity, we assumed in the model parameterization that shear-wave velocity value was increasing with depth (i.e. no velocity inversion was allowed in the Vs profile except for the pair SMA2-PAPI). The Rayleigh-wave inversion of the dispersion curves was based on a Monte Carlo sampling followed by Downhill-Simplex inversion algorithm (García-Jerez et al., 2016), for a total number of inverted models

varying from 3500 to 6500 depending on site. We plotted in Figure 13 the resulting Vs best models selected by a misfit-threshold criterium (colour scale is proportional to the misfit). The best-fit Vs models for each pair of stations, shown as red profiles in Figure 13, are plotted together in Figure 13. The Vs values of the models vary between 350 and 2000 m/s (from the uppermost meters to about 600 m deep, respectively), and the depth of the stiffer (i.e. Vs > 1000 m/s) and deeper interface is varying from 400 to 500 m (Figure 14) which could be related to the top of the Miocene Lagonegro Unit (Di Giulio et al., 2008). A further seismic contrast seems to appear in all the Vs models of Figure 14 at a depth of about 250-300 m, likely related to the Pliocenic substratum.

For the stations situated in or nearby the downtown, the interface of the deep layer is shown at about 240 m from BENI-ARC1 pair, whereas it is not clearly reached by the models obtained for GIAN-ARC1 and GIAN-CRE2. This is consistent with the shape of the experimental dispersion curves in Figure 13. The velocity models of NEW1-COST, SAB1-RUMO and SACG-GIAN are characterized by a deep stiff interface and a gradual increase of mechanical properties with depth, typical of the alluvial deposits area. According to the shape of the dispersion curve for the pair SMA2-PAPI, we allowed in this case the presence of a velocity reversal during the inversion step. The resulting velocity models at SMA2-PAPI indicate a soft layer (velocity between 350 and 600 m/s) from 40 to 130 m deep. This soft unit could be likely associated to a Pliocene silty-clay layer embedded between stiff deposits (cemented conglomerates and very dense gravels). The SMA2-PAPI pair was selected as representative of a not-normally dispersive site after a visual inspection of the dispersion curve; other curves suggest the presence of a velocity reversal in the geological structure of the city. The pairs associated to these curves do not bound a restricted sector of the city, even if are more evident for ray-paths sampling the center of the city and the south-eastern part of the investigated area. Future tomographic studies, that will follow this work, could allow the spatial identification of the areas responsible of the observed velocity inversions.

Unfortunately, independent values on the velocities for the deeper part (i.e. > 100 m) of the Benevento model are missing, and the velocity information available for the city are mostly related to microzonation studies for the uppermost 30 m of the near-surface geology (Senatore et al. 2019), in any case at a resolution scale different from that achievable with our analysis (starting from about 40 m).

7. Discussion and Conclusion

A temporary seismic network composed of 16 stations in continuous acquisition was installed in the urban area of the city. Cross-correlation of one month of ambient seismic noise was computed to reconstruct Rayleigh waves traveling between the pairs of stations. Coherent Rayleigh waves exhibit a significant energy in the frequency range 0.7–5 Hz and were used to extract the phase-velocity dispersion curves at the different station pairs. Phase velocities were measured using a strategy based on the image transformation technique developed by Yao et al. (2006). To accurately measure phase velocities of all station pairs of Benevento, up to 5 Hz, we considered also the information obtained by a constant velocity stack (CVS) analysis performed on all the ZZ components of cross-correlations. Each picked phase velocity curve was compared to velocities obtained on all cross-correlations traces to confirm the reliability of the dispersion curve and to minimize the possibility of incorrect picking. The good agreement between the dispersions estimated from standard f-k array analysis and statistical analysis of all dispersions determined by cross-correlations validates the goodness of our strategy in capturing the surface-wave phase velocities from the seismic noise. As confirmed by daily cross-correlation functions computed for each pair, the retrieved Rayleigh waves show a good stability with time. The stack of cross-correlations computed on the entire acquisition period (one month) and stack of cross-correlations computed in moving windows of different length were compared to understand how long a temporary experiment should last to provide realistic and stable results in Benevento (figure S5). In our case study, 12 days of data is enough to reproduce the cross-correlations stack computed on the

entire month of acquisition with a correlation level higher than 0.98, for all station pairs and independently of the time start of the selected window. This result cannot be directly extrapolated to other cities because it is related to the local properties of ambient seismic noise and to the Benevento subsoil structures characteristics. It is however an encouraging result that highlights a possible convenience in exporting such kind of passive seismic prospecting in other Italian cities affected by high seismic hazard.

The analyses performed on the different station pairs show an accentuate spatial variability of the dispersion curves suggesting heterogeneity of the velocity model which may be well resolved by future 3D tomographic studies. The phase-velocity dispersion curves were inverted to estimate 1D representative shear-wave velocity profiles for some areas of the city characterized by different geological units. Although we cannot perform a validation of the velocity models due to the lack of independent and a-priori information at our survey scale, the resulting models depict two main seismic interfaces, at depth of about 250 m and 400 m. The presence of a velocity reversal in the subsoil model is also retrieved by our results at different station pairs. Although such not normally dispersive curves do not identify a well defined and restricted area, they mostly affect pairs of stations connected by rays that pass through the city center and in the south-eastern part of investigated area (the area surrounding the stations CRE2, SACG and PAPI). In this latter area also Di Giulio et al. (2008) indicated velocity reversals related to the presence of ancient stiff alluvial deposits (cemented conglomerates/very dense gravels) overlaying a layer of Pliocene clays with lower velocities.

Our Vs profiles suggest a spatial heterogeneity of the shallow structure of Benevento city that extends up to ~0.5 km depth and that could have influence on seismic hazard evaluation.

In this paper we demonstrated that cross-correlation analysis of seismic noise using a small-aperture (about 4 km) array is a valid tool for the seismic characterization in urban areas like Benevento city where the high urbanization, the logistic difficulties in instruments installation make the active geophysical prospecting difficult to apply. From the inversion of the dispersion curves, estimated along several ray paths spatially distributed, is possible to reconstruct a 3D Vs model of the subsoil. 3D velocity models can be used in the urban planning within microzonation studies or in ground motion simulations contributing to risk mitigation of the cities. In this way, this kind of studies becomes an essential, non-invasive and low-cost tool in urban areas affected by high seismic hazard.

REFERENCES

Adinolfi, G. M., De Matteis, R., Orefice, A., Festa, G., Zollo, A., De Nardis, R. & Lavecchia, G., 2015. The September 27, 2012, ML 4.1, Benevento earthquake: A case of strike-slip faulting in Southern Apennines (Italy), *Tectonophysics*, **660**, 35-46, http://dx.doi.org/10.1016/j.tecto.2015.06.036.

Aki, K. 1957. Space and time spectra of stationary stochastic waves, with special reference to microtremors, *Bull. Earthq. Res. Inst.*, **35**, 415–457.

Asano, Kimiyuki, Iwata, Tomotaka, Sekiguchi, Haruko, Somei, Kazuhiro, Miyakoshi, Ken, Aoi, Shin & Kunugi, Takashi, 2017. Surface wave group velocity in the Osaka sedimentary basin,

Japan, estimated using ambient noise cross-correlation functions, *Earth, Planets and Space*, **69**. 10.1186/s40623-017-0694-3.

Bensen, G. D., Ritzwoller, M. H., Barmin, M. P., Levshin, A. L., Lin, F., Moschetti, M. P., Shapiro, N.M. & Yang, Y., 2007. Processing seismic ambient noise data to obtain reliable broad-band surface wave dispersion measurements, *Geophys. J. Int.*, **169**, 1239–1260.

Boschi, L., Weemstra, C., Verbeke, J., Ekström, G., Zunino, A. & Giardini, D., 2013. On measuring surface wave phase velocity from station–station cross-correlation of ambient signal, *Geophysical Journal International*, Volume 192, Issue 1, 1 January 2013, Pages 346–358, https://doi.org/10.1093/gji/ggs023

Di Giulio, G., Improta, L., Calderoni G. & Rovelli A., 2008. A study of the seismic response of the city of Benevento (Southern Italy) through a combined analysis of seismological and geological data, *Engineering Geology,* **97**, 146–170.

Duputel, Z., Ferrazzini, V., Brenguier, F., Shapiro, N., Campillo M. & Nercessian A., 2009. Real time monitoring of relative velocity changes using ambient seismic noise at the Piton de la Fournaise Volcano (La Réunion) from January 2006 to June 2007, *J. Volcanol. Geotherm. Res.*, **184**, 164–173

Foti, S., et al., 2018. Guidelines for the good practice of surface wave analysis: a product of the InterPACIFIC project. *Bulletin of Earthquake Engineering*, **16**(6), 2367-2420.

García-Jerez A., Piña-Flores J., Sánchez-Sesma F. J., Luzón F. & Perton M., 2016. A computer code for forward calculation and inversion of the H/V spectral ratio under the diffuse field assumption, *Computers & Geosciences*, **97**, 67–78. [doi:10.1016/j.cageo.2016.06.016].

García-Jerez A., Luzón F., Sánchez-Sesma F. J., Lunedei E., Albarello D., Santoyo M. A. & Almendros J., 2013. Diffuse elastic wavefield within a simple crustal model. Some consequences for low and high frequencies, *J. geophys. Res.*, **118**(10), 5577–5595. [doi:10.1002/2013JB010107]

Horike, M., 1985. Inversion of phase velocity of long-period microtremors to the S-wave-velocity structure down to the basement in urbanized areas, *J. Phys. Earth*., **33**, 59–96.

Konno, K. & Ohmachi, T., 1998. Ground-motion characteristics estimated from spectral ratio between horizontal and vertical components of microtremor, *Bull. seism. Soc. Am.*, **88**, 228-241.

Iannaccone, G., Improta, L., Biella, G., Castellano, M., Deschamps, A., De Franco, R., Malagnini, L., Mirabile, L., Romeo R. & Zollo A., 1995. A study of local site effects in the Benevento town (Southern Italy) by the analysis of seismic records of explosions, *Annali di Geofisica*, **38**(3–4), 411–428.

Iannaccone, G., Zollo, A., Elia, L., Convertito, V., Satriano, C., Martino, C., Festa, G., Lancieri, M., Bobbio, A., Stabile, T. A., Vassallo M. & Emolo A., 2010. A prototype system for earthquake early-warning and alert management southern Italy, *Bull. Earthq. Eng.* doi 10.1007/s10518-009-9131-8.

Improta, L., Iannaccone, G., Capuano, P., Zollo, A. & Scandone, P., 2000. Inferences on the upper crustal structure of Southern Apennines (Italy) from seismic refraction investigations and subsurface data, *Tectonophysics*, **317**(3-4), 273-298.

Improta L., Di Giulio, G. & Morelli, A., 2005. Variations of local seismic response in Benevento (Southern Italy) using earthquakes and ambient noise recordings, *J. Seismol.*, **9**(2), 191-210. DOI: 10.1007/s10950-005-3987-0

Improta, L., Ferranti, L., De Martini, P.M., Piscitelli, S., Bruno, P.P., Burrato, P., Civico, R., Giocoli, A., Iorio, M., D'Addezio, G. & Maschio, L., 2010. Detecting young, slow-slipping active faults by geologic and multidisciplinary high resolution geophysical investigations: a case study from the Apennine seismic belt, Italy, *J. geophys. Res.*, **115**, B11307. http://dx.doi.org/10.1029/2010JB000871.

Lacoss, R. T., Kelly E. J. & Toksöz M. N., 1969. Estimation of seismic noise structure using array, *Geophysics*, **34**, 21–38.

Larose, E., Derode A., Campillo M. & Fink M., 2004. Imaging from one-bit correlation of wide-band diffuse wavefield, *J. appl. Phys.*, **95**(12), 8393-8399. 10.1063/1.1739529.

Lehujeur, M., Vergne, J., Schmittbuhl, J. & Maggi, A., 2015. Characterization of ambient seismic noise near a deep geothermal reservoir and implications for interferometric methods: a case study in northern Alsace, France, *Geothermal Energy*, **3**.
DOI: http://doi.org/10.1186/s40517-014-0020-2

Levshin, A. L., Pisarenko, V. F. & Pogrebinsky, G. A., 1972. On a frequency-time analysis of oscillations, *Ann. Geophys.*, **28**(2), 211–218.

Li, H., Bernardi F. & Michelini A., 2010. Surface wave dispersion measurements from ambient seismic noise analysis in Italy, *Geophys. J. Int.*, **180**(3), 1242-1252.

Louie, J.N., 2001. Faster, Better: Shear-wave velocity to 100 meters depth from refraction microtremor arrays, *Bull. seism. Soc. Am.*, **91**(2), 347-364

Luo, Y., Yang, Y., Xu, Y., Xu, H., Zhao K. & Wang Kai, 2015. On the limitations of interstation distances in ambient noise tomography, *Geophys. J. Int.*, **201**(2), 652–661, https://doi.org/10.1093/gji/ggv043

Maresca, R., Castellano, M., De Matteis, R., Saccorotti G. & Vaccariello P., 2003. Local site effects in the town of Benevento (Italy) from noise measurements, *Pure Appl. Geophys*., **160** 1745-1764, doi:10.1007/s00024-003-2376-2.

Meletti C. & Montaldo V., 2007. Stime di pericolosità sismica per diverse probabilità di superamento in 50 anni: valori di ag. Progetto DPC-INGV S1 (2006), Deliverable D2, http://esse1.mi.ingv.it/d2.html.

McNamara, D. E. & Buland, R. P., 2004. Ambient Noise Levels in the Continental United States, *Bull. seism. Soc. Am.*, **94**(4), 1517-1527.

Milano G., Ventura, G. & Di Giovambattista R., 2004. Seismic evidence of longitudinal extension in the Southern Apennines chain (Italy): the 1997-1998 Sannio-Matese seismic sequence, *Geophys. Res. Lett.*, **29**(20), DOI 10.1029/2002GL015188.

Milano, G., Di Giovambattista R. & Ventura G., 2006. Seismicity and stress field in the Sannio–Matese area, *Ann. Geophys*., vol. **49**(1).

Molnar, S., Cassidy, J. F., Castellaro, S., Cornou, C., Crow, H., Hunter, J. A., Matsushima, S., Sánchez-Sesma, F. J. & Yong A., 2018. Application of Microtremor Horizontal-to-Vertical Spectral Ratio (MHVSR) Analysis for Site Characterization: State of the Art. *Surveys in Geophysics*, 1-19. https://doi.org/10.1007/s10712-018-9464-4

Nunziata, C., De Nisco G. & Panza G. F., 2009. S-waves profiles from noise cross correlation at small scale, *Engineering Geology*, **105**(3), 161-170.

Obermann, A., Kraft, T. Larose E. & Wiemer S., 2015. Potential of ambient seismic noise techniques to monitor the St. Gallen geothermal site (Switzerland), *J. Geophys. Res. Solid Earth*, **120**, 4301–4316. doi:10.1002/2014JB011817.

Pastén, C., Sáez, Ruiz, M., Leyton, F., Salomon J. & Poli P., 2016. Deep characterization of the Santiago Basin using HVSR and cross-correlation of ambient seismic noise, *Eng. Geol*., **201**, 57-66.

Park, C.B., Miller, R. D. & Xia, J., 1999. Multichannel analysis of surface waves, *Geophysics*, **64**(3), 800-808

Pescatore, T., Improta, L., Romeo R. & Iannaccone G., 1996. Geologia della città di Benevento: caratteristiche litostratigrafiche finalizzate alla microzonazione sismica, *Boll. Soc. Geol. Ital.*, **115**.

Pescatore, T., Senatore M. R. & Boscaino M., 2005. La geologia di Benevento: un modello fisico del sottosuolo per lo studio della risposta sismica, Convegno Nazionale GNDT, Ext. Abst., Genova 15-16 February 2005.

Peterson, J., 1993. Observation and modeling of seismic background noise, U.S. Geol. Surv. Open-File Rept. 93-322

Piña-Flores J., Perton M., García-Jerez A., Carmona E., Luzón F., Molina-Villegas J. C. & Sánchez-Sesma F. J., 2017. The inversion of spectral ratio H/V in a layered system using the diffuse field assumption (DFA), *Geophys. J. Int*., **208**, 577-588. [doi:10.1093/gji/ggw416]

Picozzi, M., Parolai, S., Bindi D. & Strollo A., 2009. Characterization of shallow geology by high-frequency seismic noise tomography, *Geophys. J. Int.*, **176**, 164-174.

Pilz, M., Parolai S. & Bindi D., 2013. Three-dimensional passive imaging of complex seismic fault systems: evidence of surface traces of the Issyk-Ata fault (Kyrgyzstan), *Geophys. J. Int*., **194**(3), 1955-1965, doi: 10.1093/gji/ggt214.

Renalier, F., Jongmans, D., Savvaidis, A., Wathelet, M., Endrun, B. & Cornou, C., 2010. Influence of parameterization on inversion of surface wave dispersion curves and definition of an inversion strategy for sites with a strong Vs contrast. *Geophysics*, **75**(6), B197-B209.

Rovida, A., Camassi, R., Gasperini P. & Stucchi M., 2011. CPTI11, the 2011 Version of the Parametric Catalogue of Italian Earthquakes. http://dx.doi.org/10.6092/INGV.IT-CPTI11 (Milano, Bologna,http://emidius.mi.ingv.it/CPTI).

Roux, P., 2009. Passive seismic imaging with directive ambient noise: application to surface waves and the San Andreas Fault in Parkfield. CA., *Geophys. J. Int.*, 367–373.

Sadeghisorkhani, H., Gudmundsson, O. & Tryggvason, A., 2018. GSpecDisp: A matlab GUI package for phase-velocity dispersion measurements from ambient-noise correlations, *Computers & Geosciences*, **110**, 41-53, ISSN 0098-3004, https://doi.org/10.1016/j.cageo.2017.09.006.

Sánchez-Sesma, F. J. & Campillo M., 2006. Retrieval of the Green's Function from Cross Correlation: The Canonical Elastic Problem, *Bull. seismo. Soc. Am.*, **96**(3), 1182-1191.

Sánchez-Sesma F.J., Rodríguez M., Iturrarán-Viveros U., Luzón F., Campillo M., Margerin L., García-Jerez A., Suarez M., Santoyo M. A. & Rodríguez-Castellanos A., 2011. A theory for microtremor H/V spectral ratio: application for a layered medium, *Geophys. J. Int*., **186**, 221–225. [doi:10.1111/j.1365-246X.2011.05064.x]

Senatore, M. R., Boscaino M. & Pinto F., 2019. The quaternary geology of the Benevento urban area (southern Italy) for seismic microzonation purposes, *Ital. J. Geosci*., **138**, 66-87, https://doi.org/10.3301/IJG.2018.27

Shapiro, N. M., Campillo, M., Stehly L. & Ritzwoller M., 2005. High- Resolution Surface-Wave tomography from ambient seismic noise, *Science*, **307**, 1615–1618.

Shirzad, T. & Shomali Z. H., 2015). Extracting Seismic Body and Rayleigh Waves from the Ambient Seismic Noise Using the rms- Stacking Method, *Seismol. Res. Lett.*, **86**, 173-180, doi: 10.1785/0220140123

Vassallo, M., Festa G. & Bobbio A., 2012. Seismic Ambient Noise Analysis in Southern Italy, *Bull. seismo. Soc. Am*., **102**(2), 574–586, doi: 10.1785/0120110018.

Vassallo, M., Festa, G., Bobbio A. & Serra M., 2016. Low shear velocity in a normal fault system imaged by ambient noise cross correlation: The case of the Irpinia fault zone, Southern Italy, *J. Geophys. Res. Solid Earth*, **121**, doi:10.1002/2015JB012410.

Vilardo G., Nappi, R., Petti P. & Ventura G., 2003. Fault geometries from the space distribution of the 1990-1997 Sannio-Benevento earthquakes: inferences on the active deformation in Southern Apennines, *Tectonophysics*, **363**(3-4), 259-271.

Wiggins R. A., 1976. Interpolation of digitized curves., *Bull. seismo. Soc. Am*., **66**(6), 2077–2081.

Yao, H., Van Der Hilst R.D. & de Hoop, M. V., 2006. Surface-wave array tomography in SE Tibet from ambient seismic noise and two-station analysis : I - Phase velocity maps. *Geophys. J. Int.*, **166**(2), 732-744, doi: 10.1111/j.1365-246X.2006.03028.x**.**

Yilmaz, O., 1987. Seismic data processing, in Doherty, S. M., and Neitzel, E. B., series Eds., Investigations in geophysics, 2: Soc. Expl. Geophys.

Xia J., Miller R.D. & Park C.B., 1999. Estimation of near-surface shear-wave velocity by inversion of Rayleigh waves, *Geophysics*, **64**(3), 691-700.

Table1: *Temporary seismic network installed in Benevento city, list of seismic stations.*

STAZ.	LAT. N (°)	LON. E (°)	DIGITIZER	SENSOR	SAMPLING RATE (Hz)	Bandwidth
DEFI	41.1224	14.78935	CENTAUR	TRILLIUM COMPACT 120s	100	120s-50Hz
GIAN	41.130534	14.78562	CENTAUR	TRILLIUM COMPACT 120s	100	120s-50Hz
PAPI	41.11635	14.8005	CENTAUR	TRILLIUM COMPACT 120s	100	120s-50Hz
PAX1	41.13545	14.78890	CENTAUR	TRILLIUM COMPACT 120s	100	120s-50Hz
RUMO	41.118496	14.777556	Q330	LE3D 5s	100	5s-50Hz
SACG	41.123610	14.797961	Q330	LE3D 5s	100	5s-50Hz
COST	41.136782	14.773503	Q330	LE3D 5s	100	5s-50Hz
SMA1	41.126732	14.779156	Q330	LE3D 5s	100	5s-50Hz
SPSA	41.146873	14.780036	Q330	LE3D 5s	100	5s-50Hz
NEW1	41.140571	14.787799	Q330	LE3D 5s	100	5s-50Hz
SMA2	41.126060	14.783042	Q330	LE3D 5s	100	5s-50Hz
CAL1	41.134542	14.770399	Q330	LE3D 5s	100	5s-50Hz
SAB1	41.125536	14.768545	Q330	LE3D 5s	100	5s-50Hz
ARC1	41.131775	14.778517	Q330	LE3D 5s	100	5s-50Hz
CRE2	41.129241	14.791881	Q330	LE3D 5s	100	5s-50Hz
BENI	41.129799	14.771600	D6BB-DIN	EPISENSOR FBA ES-T	125	DC-200Hz

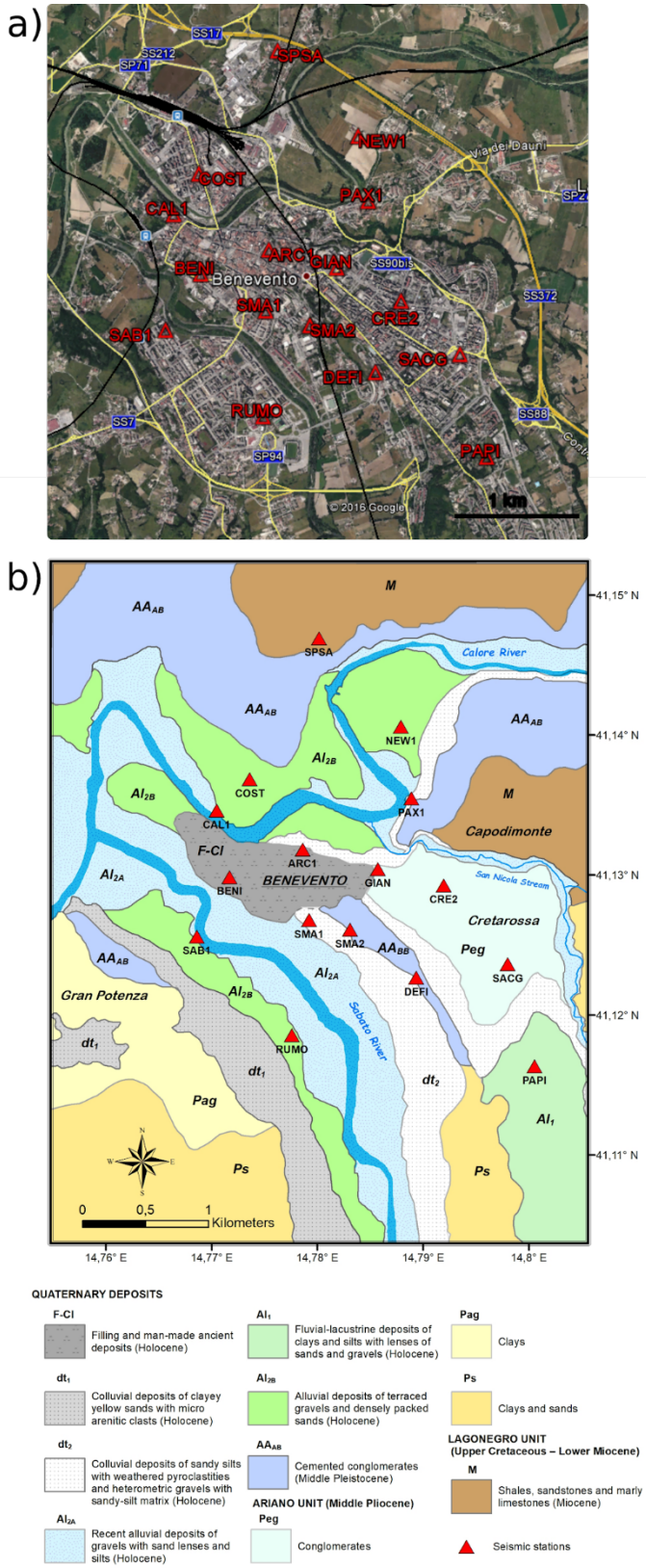

Figure 1: *a) Seismic network installed in the Benevento city (Southern Italy). Red triangles indicate the position of seismic stations, the yellow lines show the main roads and the black lines the railways of the city. b) geological map (redrawn from Improta et al., 2005).*

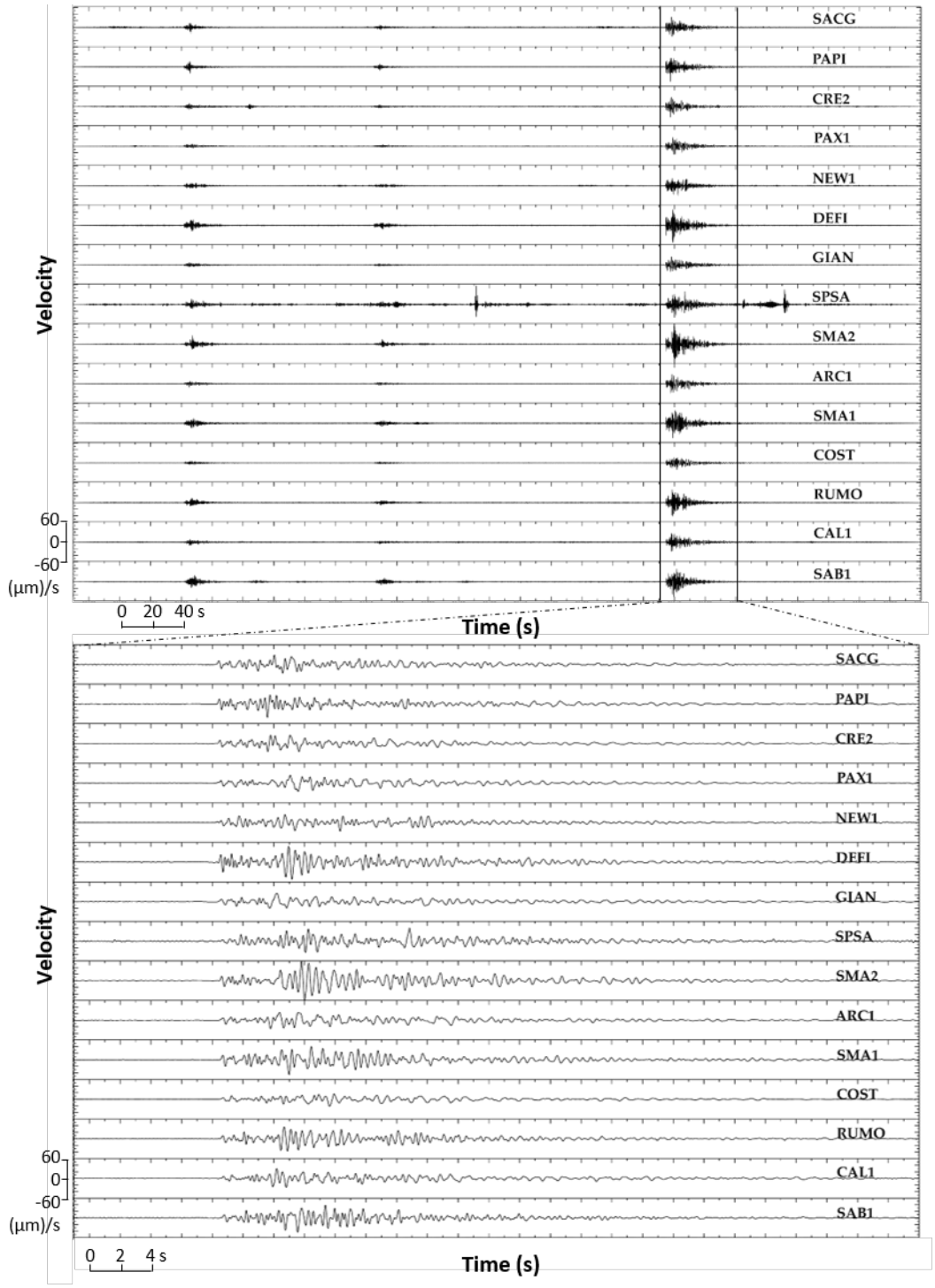

Figure 2: *Top: three events of a seismic sequence recorded at stations of Benevento temporary network. Bottom: the 2.7 magnitude event recorded at stations installed in Benevento city.*

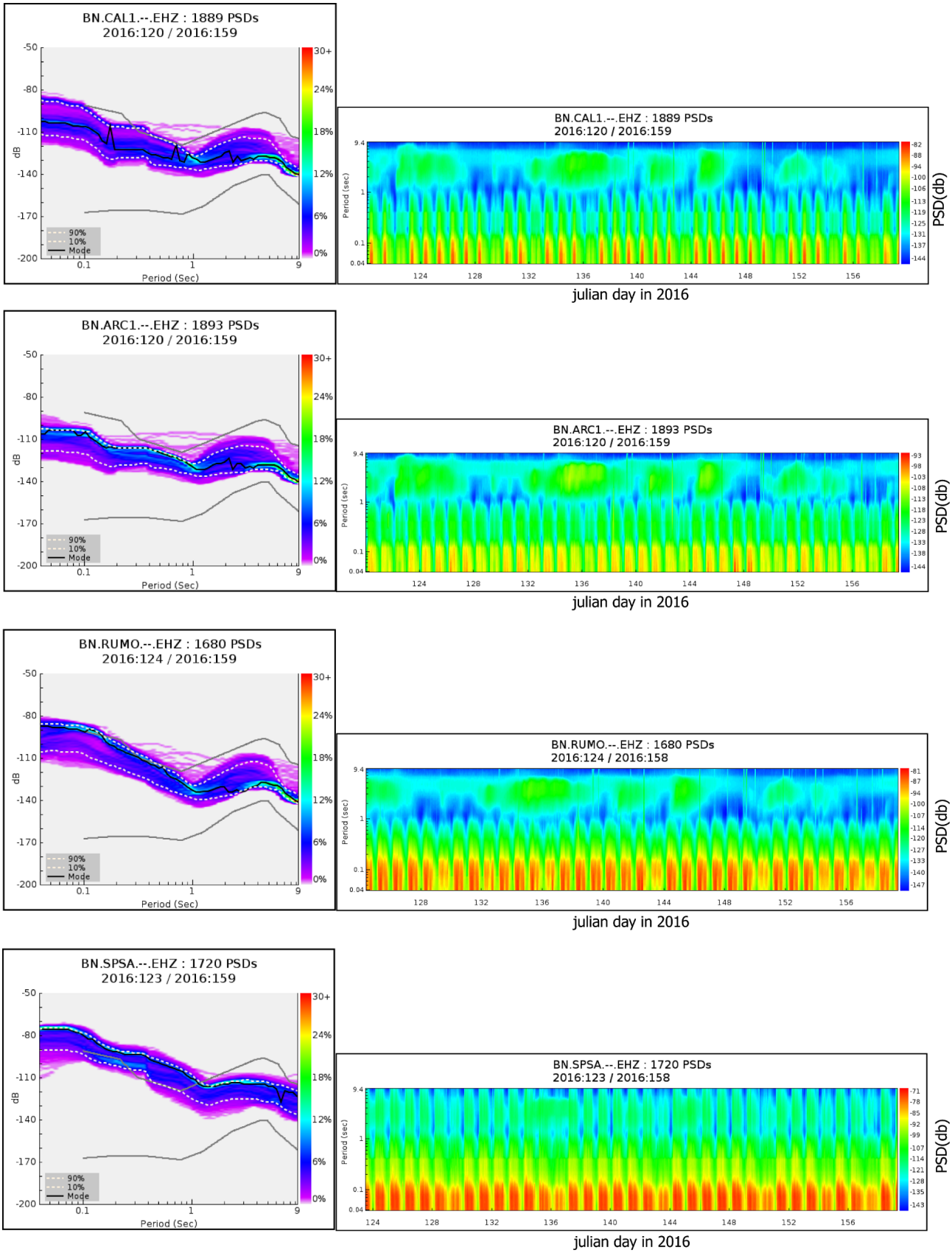

Figure 3: *On the left the Probability Density Function from continuous seismic noise recorded by four station (vertical components) of Benevento Temporary network for a 30 days acquisition period. Color bar: probability. Black curve: mode. White dotted lines: 10th and 90th percentile. Gray lines: Peterson reference lines. On the right the related spectrograms.*

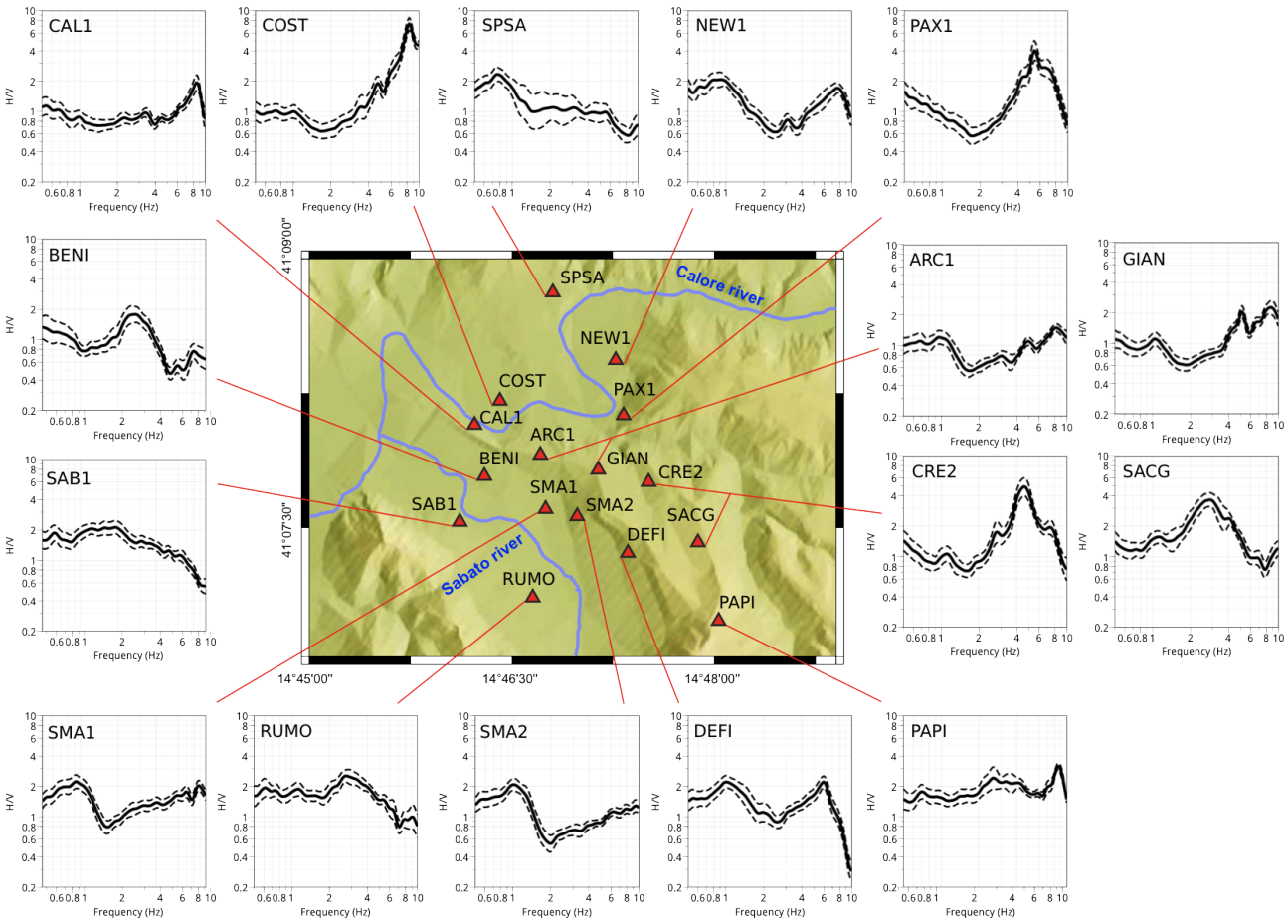

Figure 4: *H/V noise spectral ratios computed on time-window length of 1 day. Average H/V spectral ratio (solid line) is represented along with standard deviation (dashed lines).*

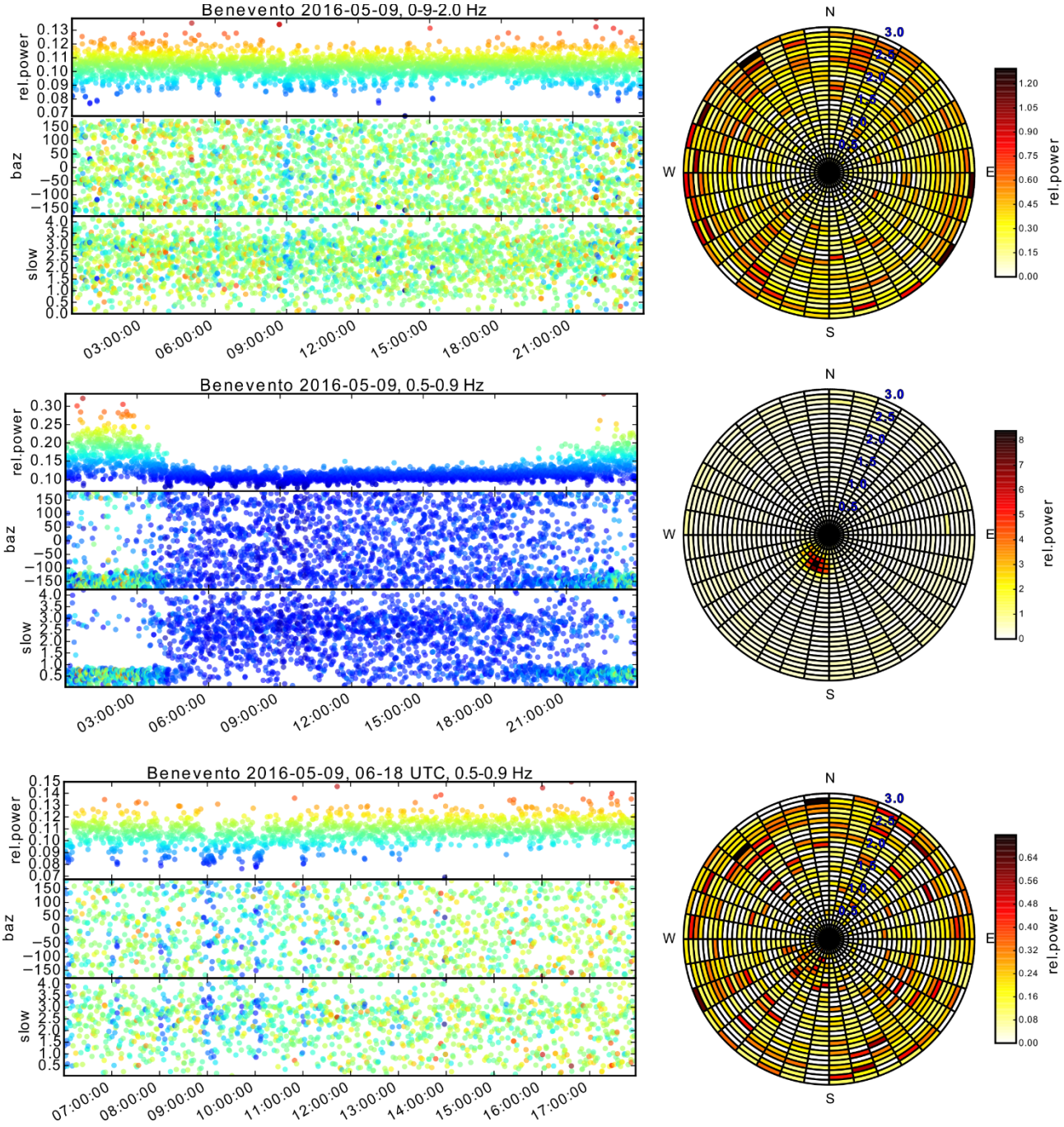

Figure 5: *The figure shows the beamforming results obtained using the Benevento data acquired on 2016/05/09 in two different frequency bands (a: 0.9-2.0 Hz; b: 0.5-0.9 Hz). In c) there is a zoomed view of b) between the 06:00 and 18:00. The beamforming results are shown in two different representations. The first one shows the time evolution of relative power, backazimuth and slowness. The same estimations are represented in a polar plot which sums the relative power in gridded bins (angular and slowness step of 10° and in 0.1 i/m, respectively).*

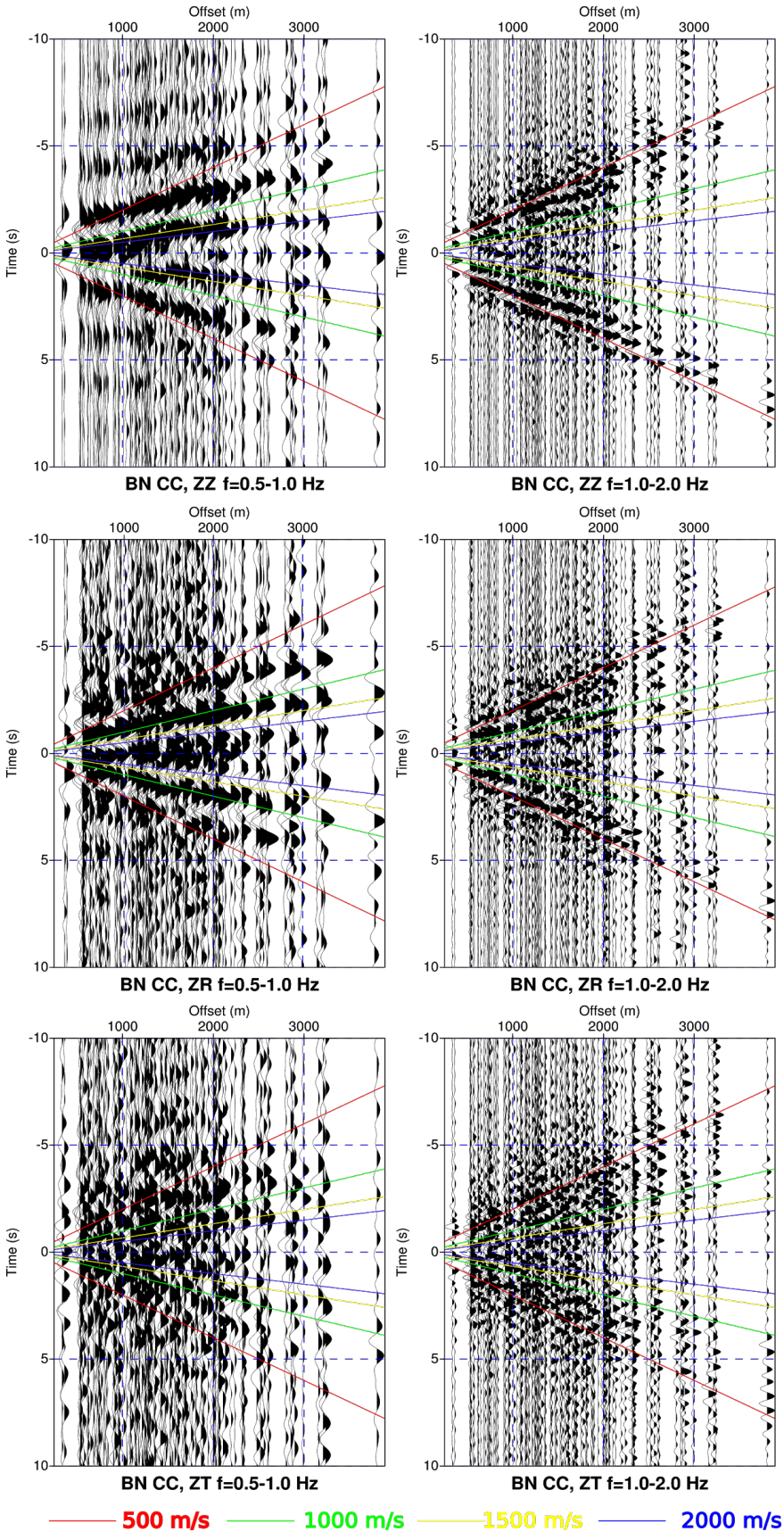

Figure 6: *Cross-correlation stacks for three (ZZ, ZR, ZT) components of the correlation tensor, organized for increasing interstation distance and computed in two different frequency bands. Each trace is normalized to its maximum value. The components and frequency bands are indicated below each seismic section. The blue, yellow, green and red lines show the theoretical arrival times of a surface wave with velocity of 2000, 1500, 1000 and 500 m/s, respectively.*

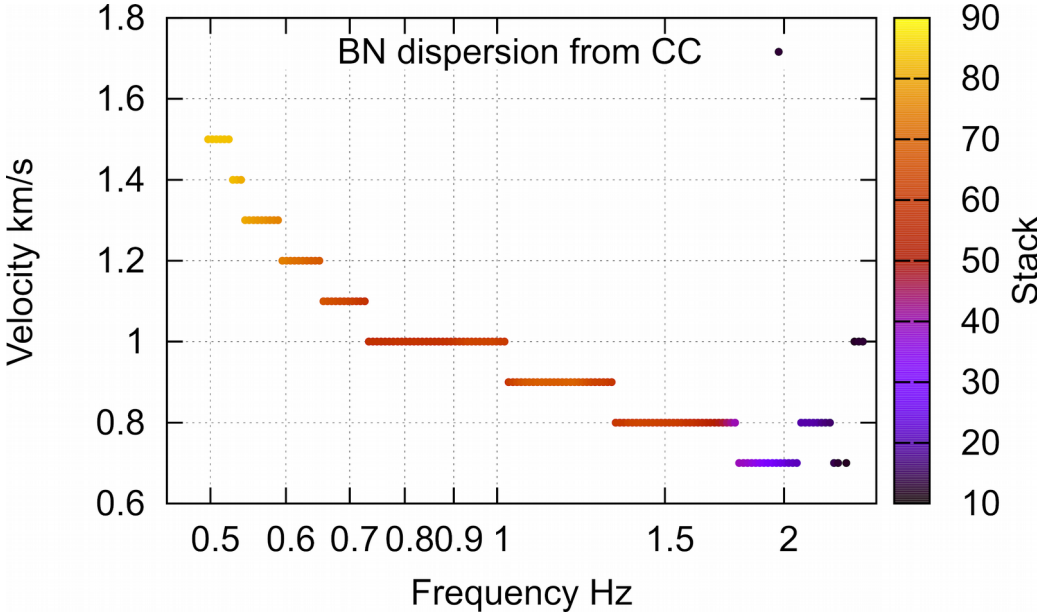

Figure 7: *Results of velocity analysis performed on ZZ component of all computed cross-correlations. For each analyzed frequency the point represents the surface velocity correction which maximizes the stack function. The color of points is linked to the stack value defined between 0 and 120 (all corrected traces aligned).*

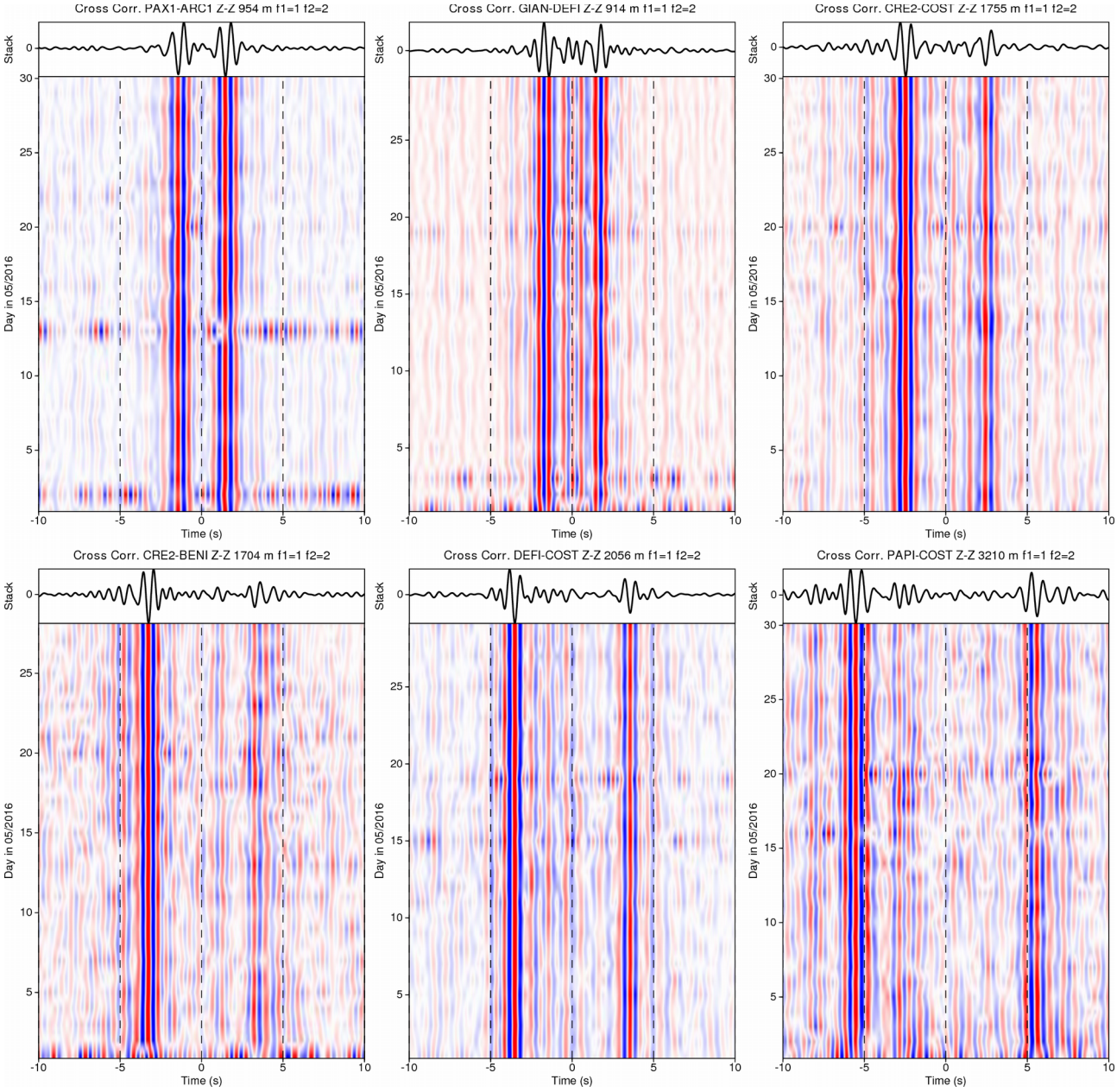

Figure 8: *Cross-correlations filtered between 1Hz and 2Hz for six pairs of stations (PAX1-ARC1, GIAN-DEFI, CRE2-COST, CRE2-BENI, DEFI-COST, and PAPI-COST) as a function of time computed with data acquired in May 2016. Each trace represents the cross-correlation for 24 h long signals, and it's plotted in a color scale where blue and red indicate positive and negative amplitudes, respectively. For each pair, the stack of all the cross-correlation functions is highlighted on top of the related panel.*

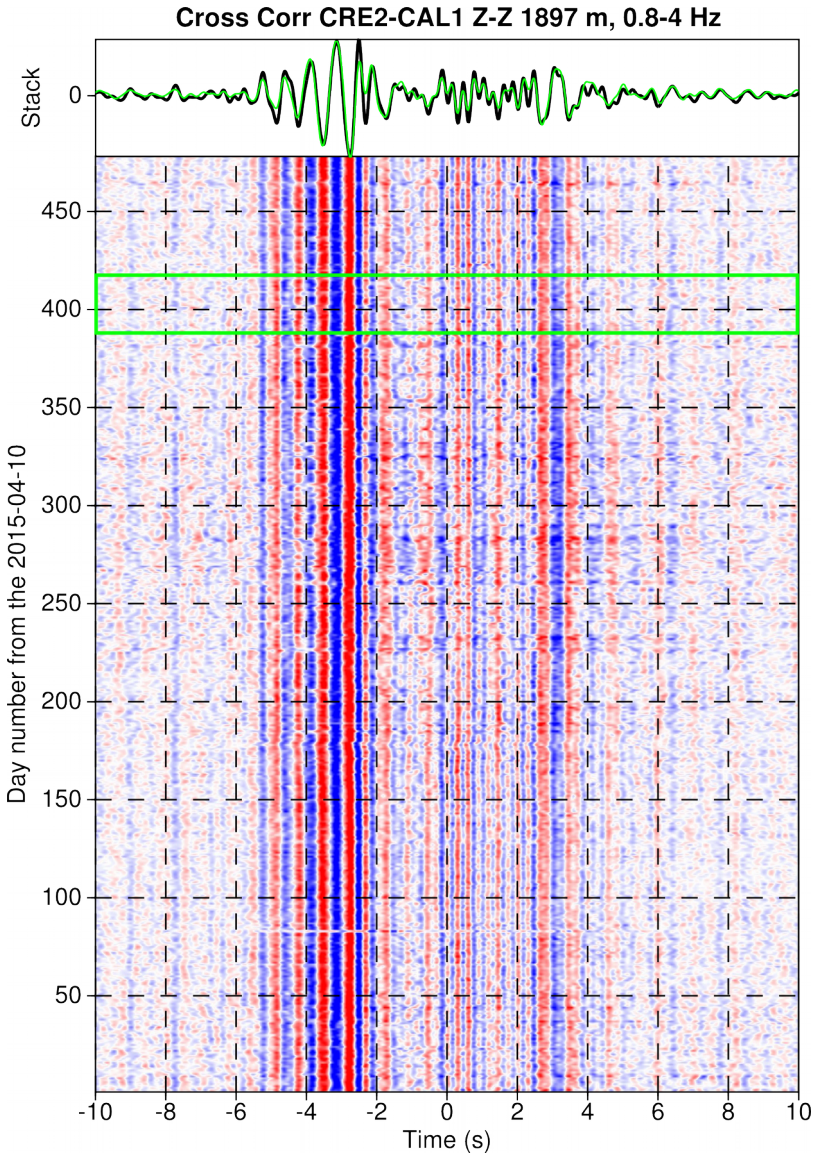

Figure 9: *Cross-correlations in 0.8-4Hz for CRE2-CAL1 as a function of time starting from 2015-04-10. The data in the green box are related to the duration of the experiment as described in the manuscript. On top, the stack trace computed using all the data (black trace) is compared with the stack computed with data acquired during one month of the experiment (green trace).*

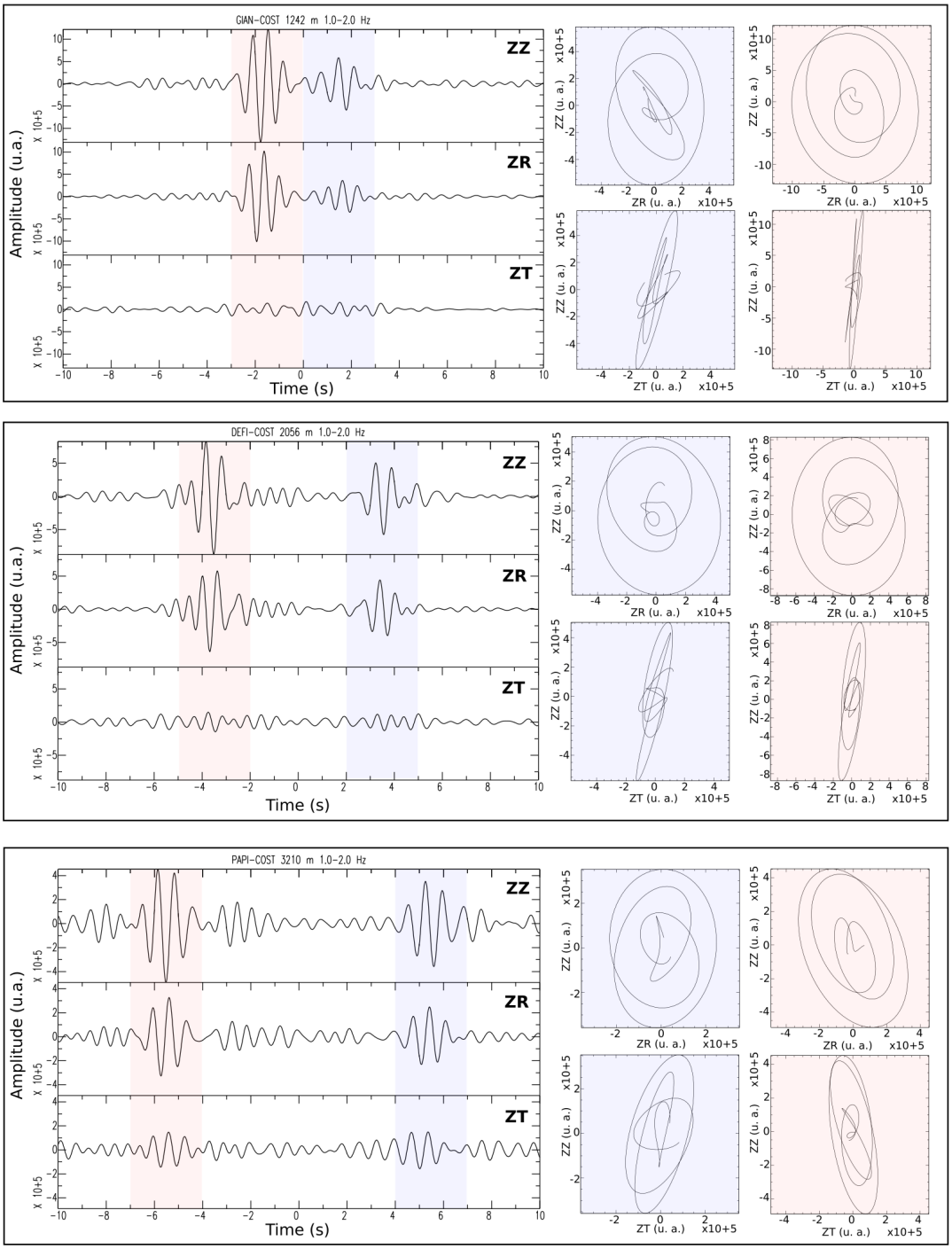

Figure 10: *Three components of cross-correlation tensor (ZZ, ZR, ZT) computed for three pair of stations (GIAN-COST, DEFI-COST, PAPI-COST) and its related particle motion. For each pair the ZZ, ZR and ZT components of cross-correlations are shown together with particle motion plot of the stacked cross-correlations. In each analyzed case, the particle motion is restricted mainly to the Z-R plane, where it exhibits the elliptical motion characteristic of Rayleigh waves. This characteristic is consistent for particle motion computed using causal (azure panels) and acausal (pink panels) selected signals within the azure and pink boxes present in the three components of cross-correlations.*

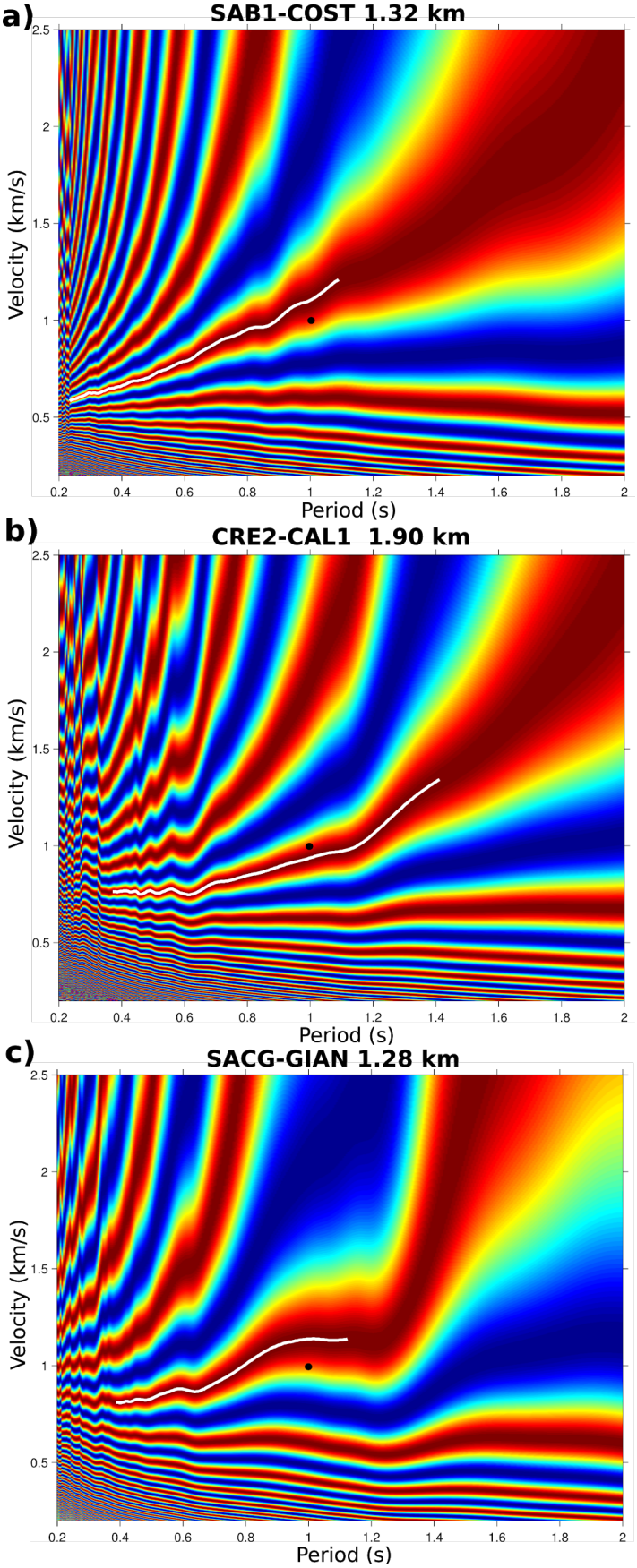

Figure 11: *Phase velocity dispersion measurements from the ZZ component of SAB1-COST1, CRE2-CAL1, SACG-GIAN cross-correlations. For each pair the phase velocity-period image is used to define the dispersion curves (white lines). The black point represents the velocity value extracted by fig. 8 and is used to determine the branch to follow for the dispersion curve determination.*

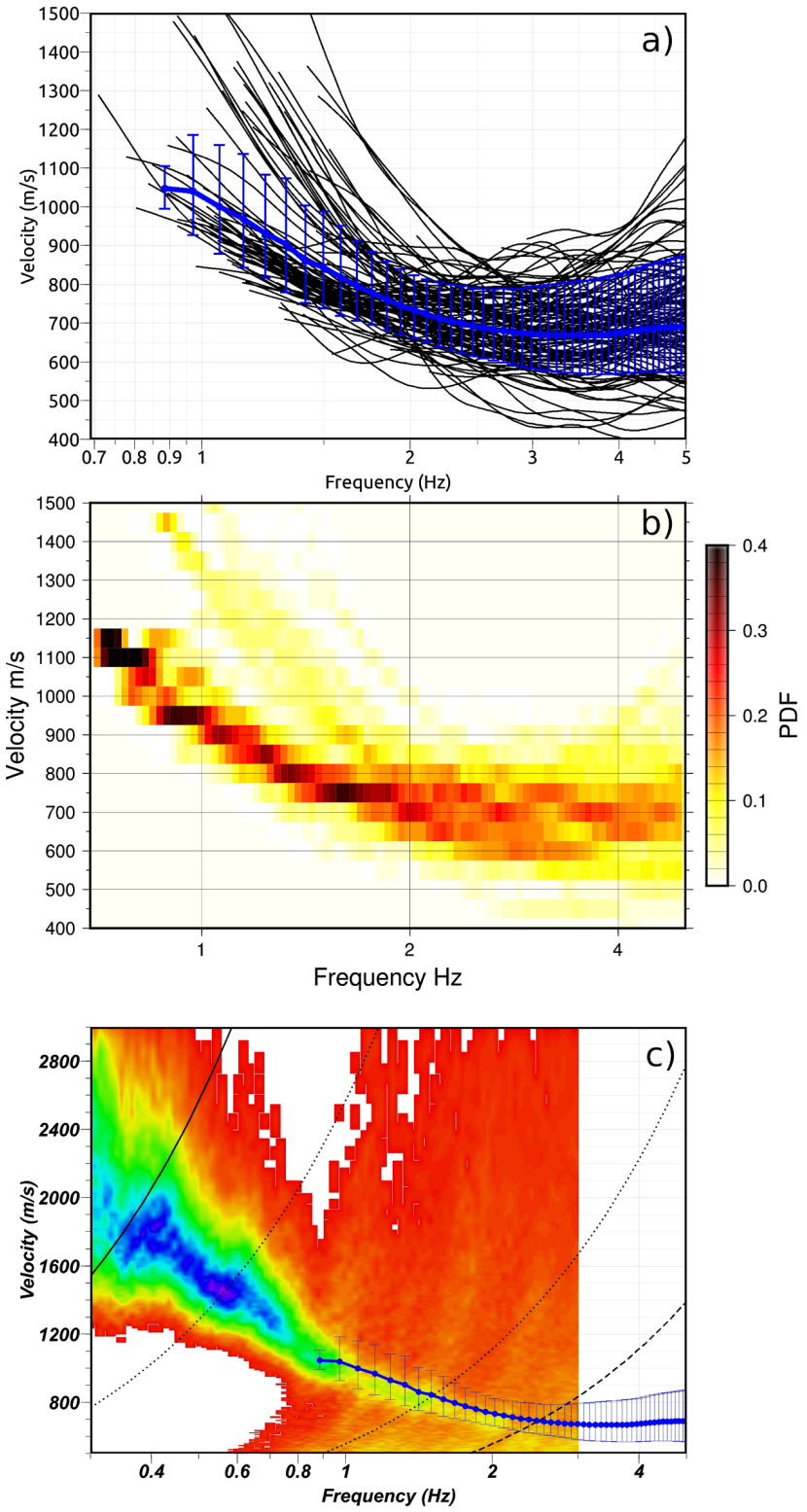

Figure 12: *a) Phase dispersion curves (black lines) from the ZZ cross-correlations of 115 station pairs and averaged curve with standard deviations (blue line). b) Probability density function of phase velocity in Benevento computed using all the estimated dispersion curves. c) Comparison between standard f-k results and average dispersion curves from cross-correlation picking. The colour scale is proportional to the beam power and the resolution and alias limits of the array are shown as thin black curves. The blue line represents the average dispersion curves and standard deviation obtained by dispersion curves at the different stations pairs (panel a).*

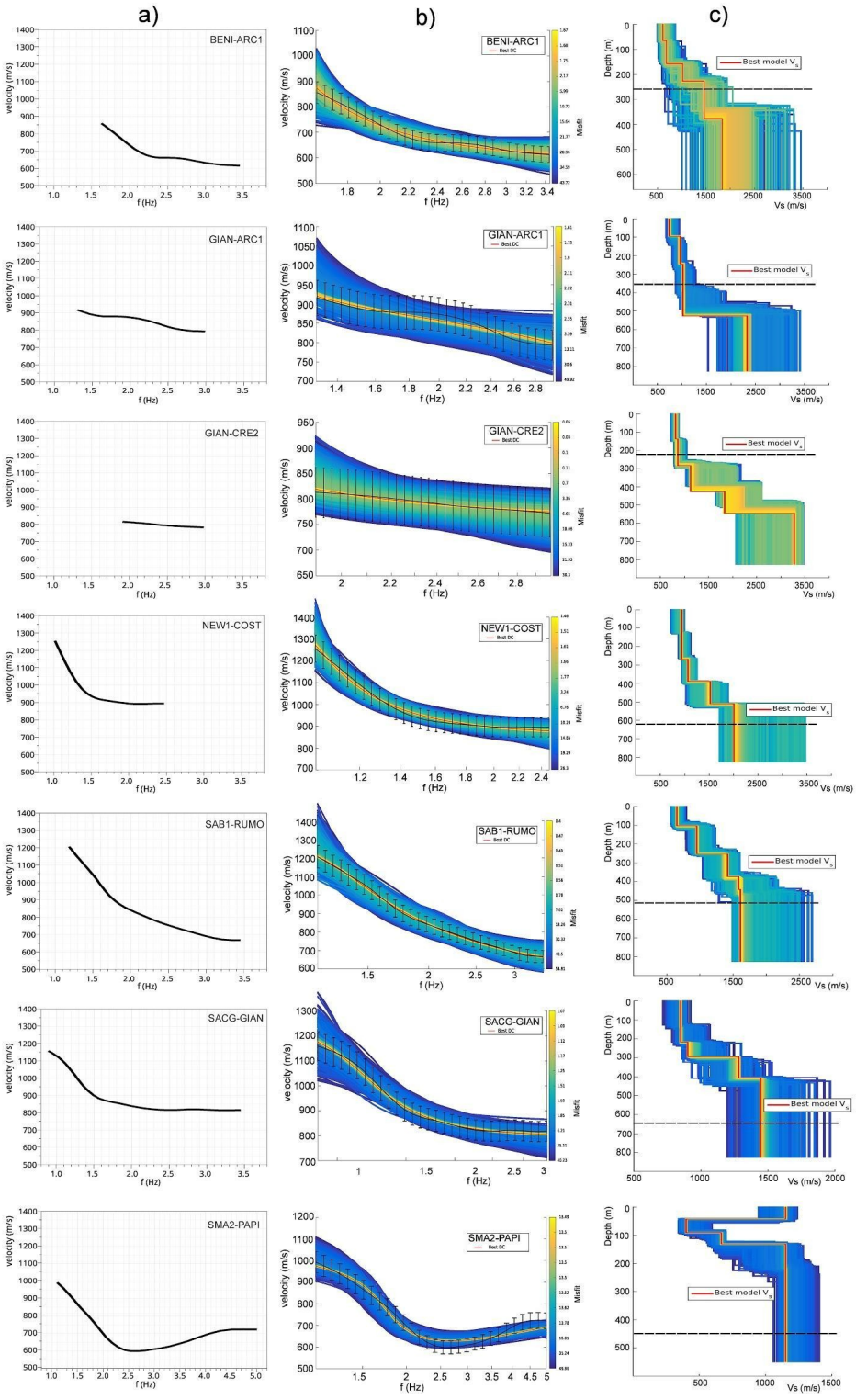

Figure 13: *a) Dispersion curves obtained by the cross-correlation analysis (see also Fig. 11) for seven pairs of stations (BENI-ARC1, GIAN-ARC1, GIAN-CRE2, NEW1-COST, SAB1-RUMO, SACG-GIAN and SMA2-PAPI). b) Inverted models in terms of dispersion curves of Rayleigh surface-wave fundamental mode. The measured dispersion curve is the black curve (shown also in panel a), the dispersion models are shown in colour that is proportional to the misfit after the inversion procedure. c) Inverted models in terms of Vs profiles. The best-fit Vs model is shown as red curve. The vertical dashed line is the maximum depth of investigation estimated as half of the maximum wavelength.*

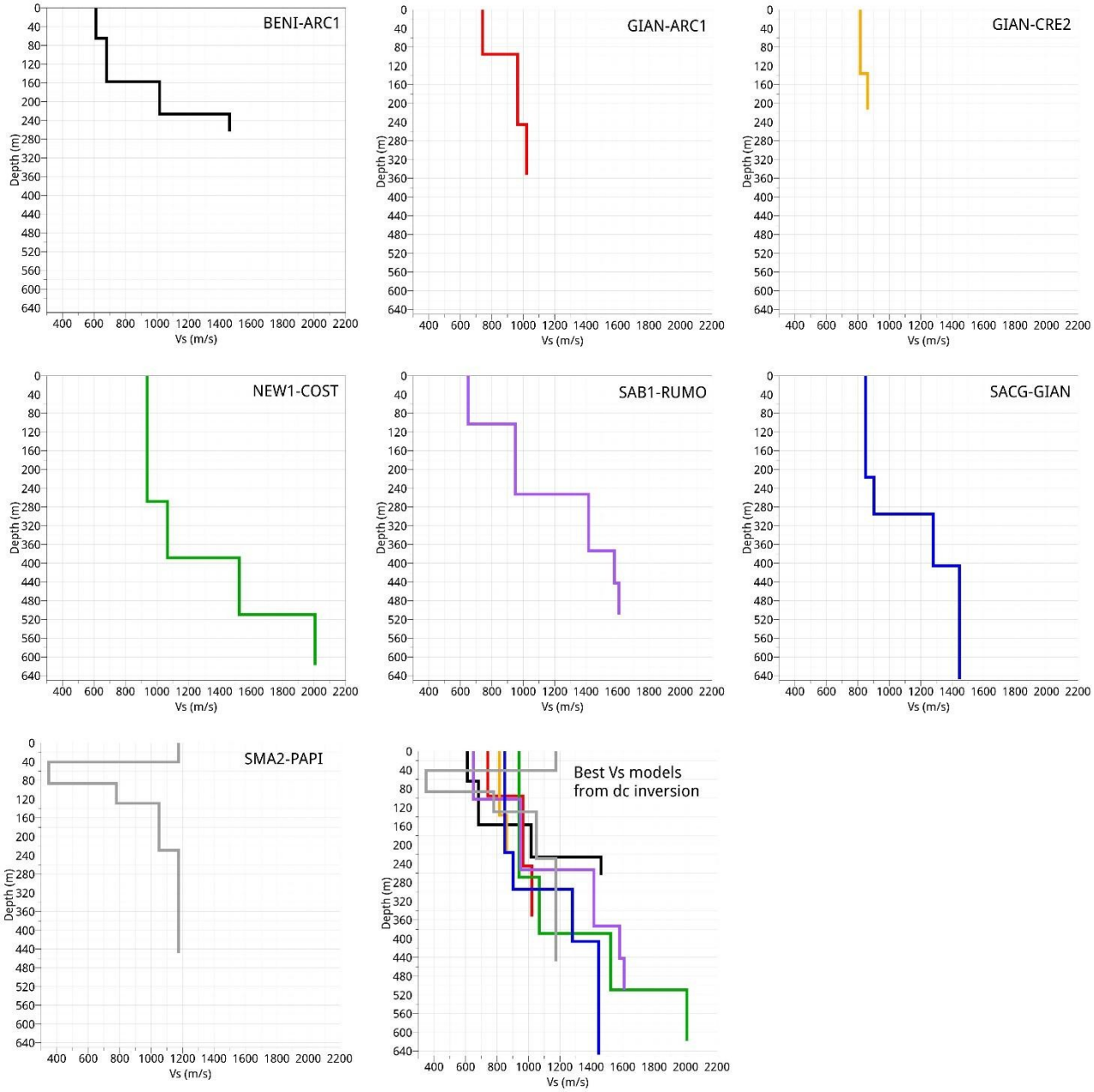

Figure 14: *Comparison of the best-fit Vs models (red curves in Fig. 13) for the seven pairs of stations.*

Supporting Information for

Seismic noise cross-correlation in the urban area of Benevento city (Southern Italy)

Maurizio Vassallo[1], Raffaella De Matteis[2], Antonella Bobbio[3], Giuseppe Di Giulio[1], Guido Maria Adinolfi[4], Luciana Cantore[1*], Rocco Cogliano[5], Antonio Fodarella[5], Rosalba Maresca[2], Stefania Pucillo[5], Gaetano Riccio[5]

[1] Istituto Nazionale di Geofisica e Vulcanologia, Viale Francesco Crispi 43/47, 67100, L' Aquila, Italy.
[2] Dipartimento di Scienze e Tecnologie, Università degli Studi del Sannio, Via dei Mulini, 82100 Benevento, Italy
[3] Istituto Nazionale di Geofisica e Vulcanologia - Osservatorio Vesuviano, Via Diocleziano, 328, 80145 Napoli, Italy
[4] Dipartimento di Fisica, Università degli Studi di Napoli Federico II, Complesso Universitario di Monte S.Angelo, Via Cinthia, 80124 Napoli, Italy
[5] Istituto Nazionale di Geofisica e Vulcanologia, c.da Ciavolone, Grottaminarda 83035, Avellino, Italy.
[*] Now at Ministero dell'Istruzione dell'Università e della Ricerca.

Corresponding author
Maurizio Vassallo
Istituto Nazionale di Geofisica e Vulcanologia, Viale Francesco Crispi 43/47, 67100, L' Aquila, Italy
email: maurizio.vassallo@ingv.it
+39 0862709120

Contents of this file

Figures S1 to S6

Introduction

This supporting information provides 6 extra-figures that can help the reader in understanding some of the concepts contained in the manuscript.

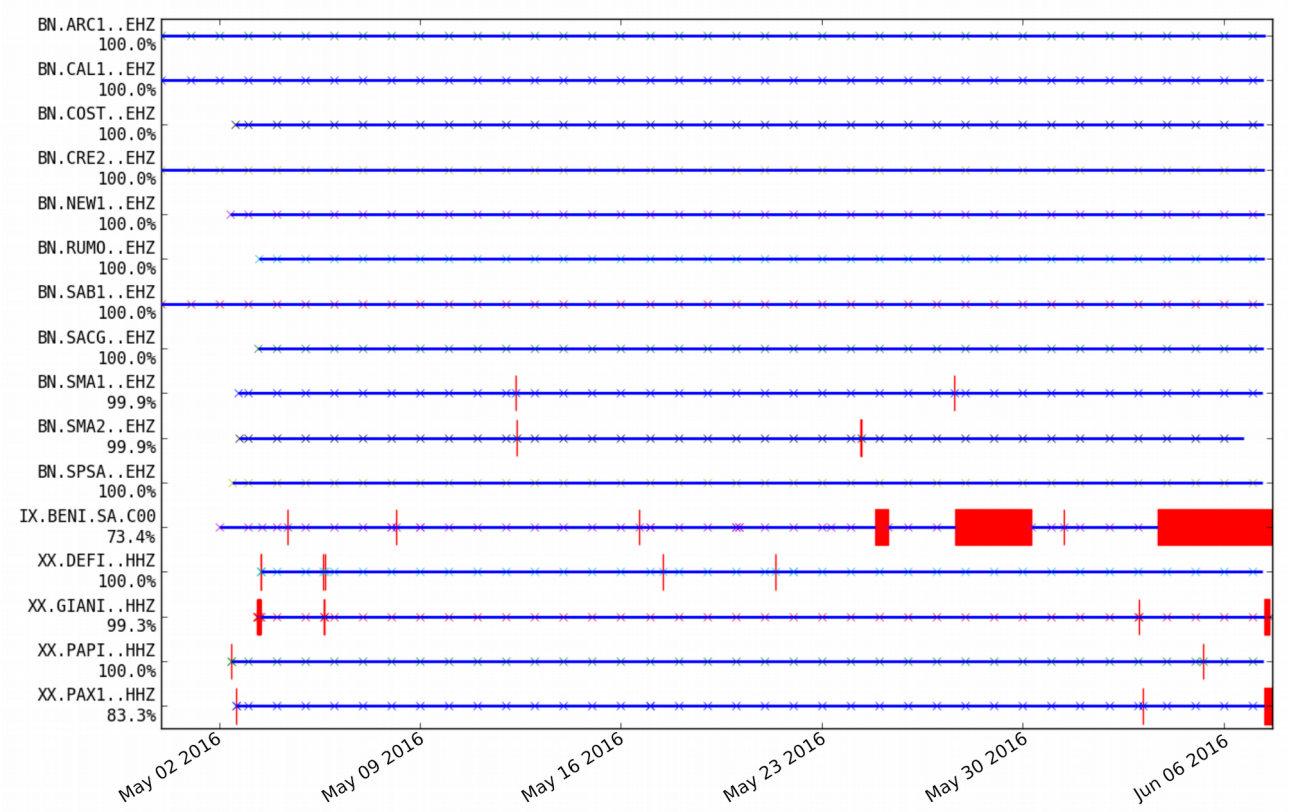

Figure S1: Data availability of the Benevento temporary seismic network composed by 16 stations in continuous acquisition for about 37 days. The data coverage for each station is represented in a separate horizontal line. Gaps in data availability are indicated by vertical red lines.

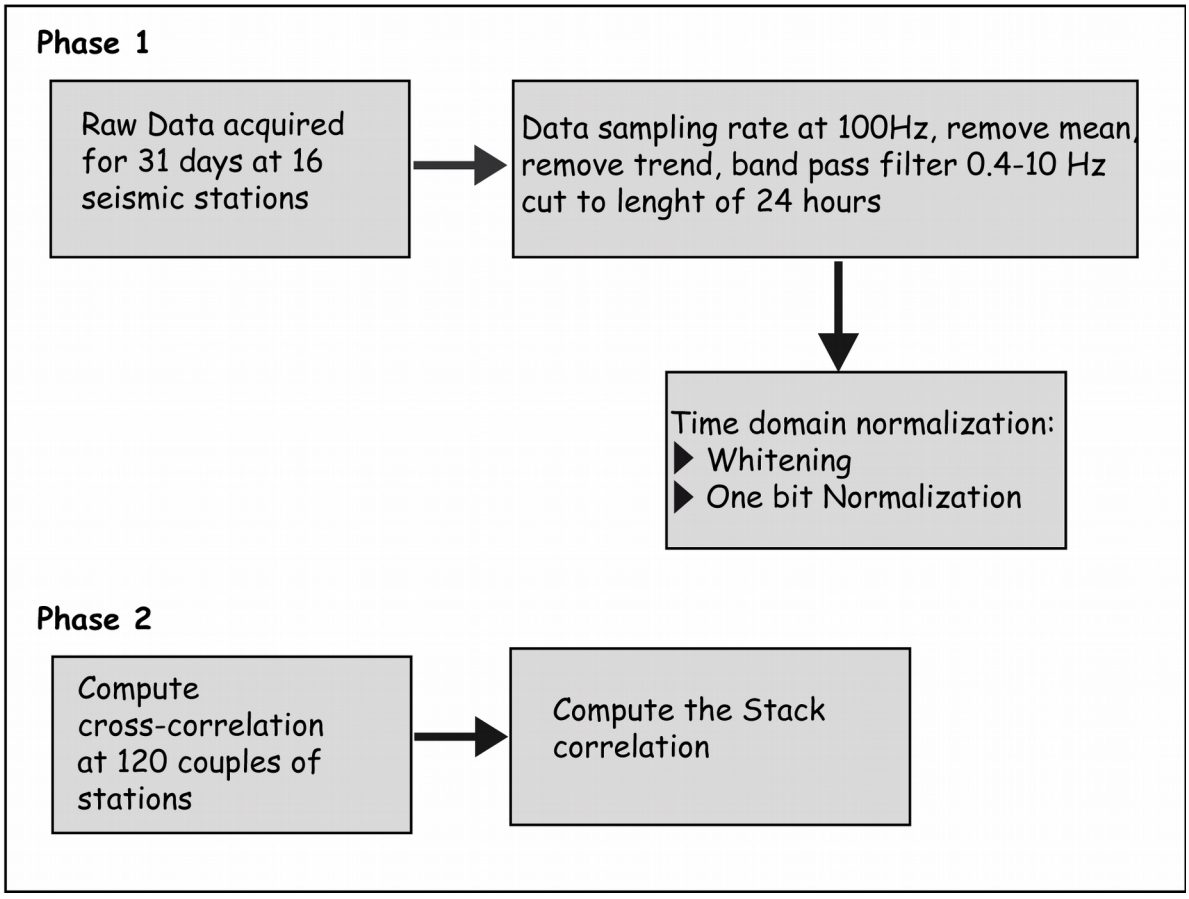

Figure S2: Block scheme for single-station (Phase 1) and cross-correlation processing (Phase 2). After data selection and filtering, data are equalized in time domain by one-bit normalization resulting into a barcode signal that keeps only phase information. In the Phase 2 the normalized traces are cross correlated for pairs of stations and stacked.

Figure S3: Comparison between the phase dispersion curves obtained by the method proposed in this work (called as Yao's method, red curves) and by the method based on the zero crossing of the real part of correlation spectrum (called as Aki's method, green curves).

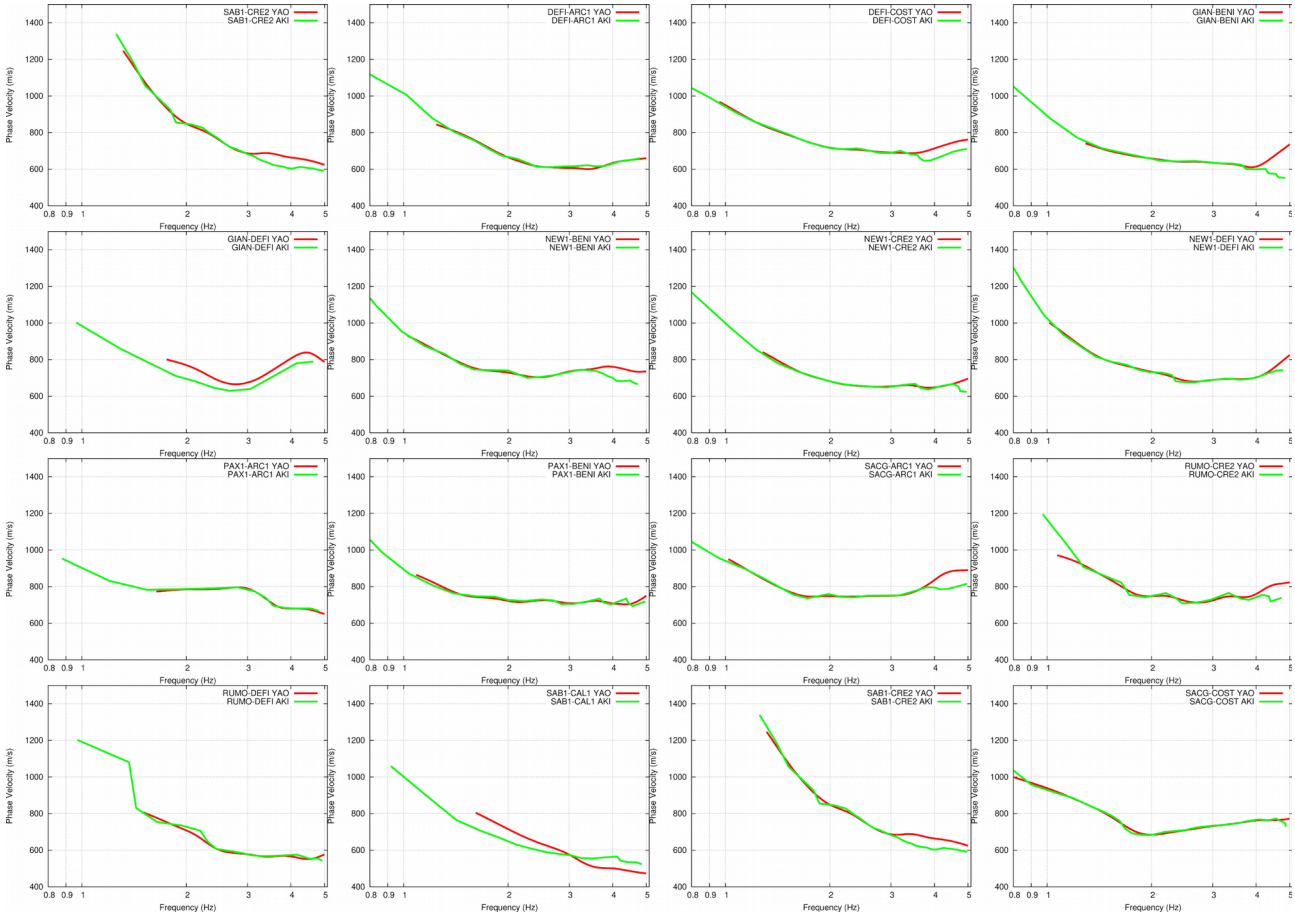
SAB1-CRE2 YAO
SAB1-CRE2 AKI
DEFI-ARC1 YAO
DEFI-ARC1 AKI
DEFI-COST YAO
DEFI-COST AKI
GIAN-BENI YAO
GIAN-BENI AKI
GIAN-DEFI YAO
GIAN-DEFI AKI
NEW1-BENI YAO
NEW1-BENI AKI
NEW1-CRE2 YAO
NEW1-CRE2 AKI
NEW1-DEFI YAO
NEW1-DEFI AKI
PAX1-ARC1 YAO
PAX1-ARC1 AKI
PAX1-BENI YAO
PAX1-BENI AKI
SACG-ARC1 YAO
SACG-ARC1 AKI
RUMO-CRE2 YAO
RUMO-CRE2 AKI
RUMO-DEFI YAO
RUMO-DEFI AKI
SAB1-CAL1 YAO
SAB1-CAL1 AKI
SAB1-CRE2 YAO
SAB1-CRE2 AKI
SACG-COST YAO
SACG-COST AKI
Phase Velocity (m/s)
Frequency (Hz)

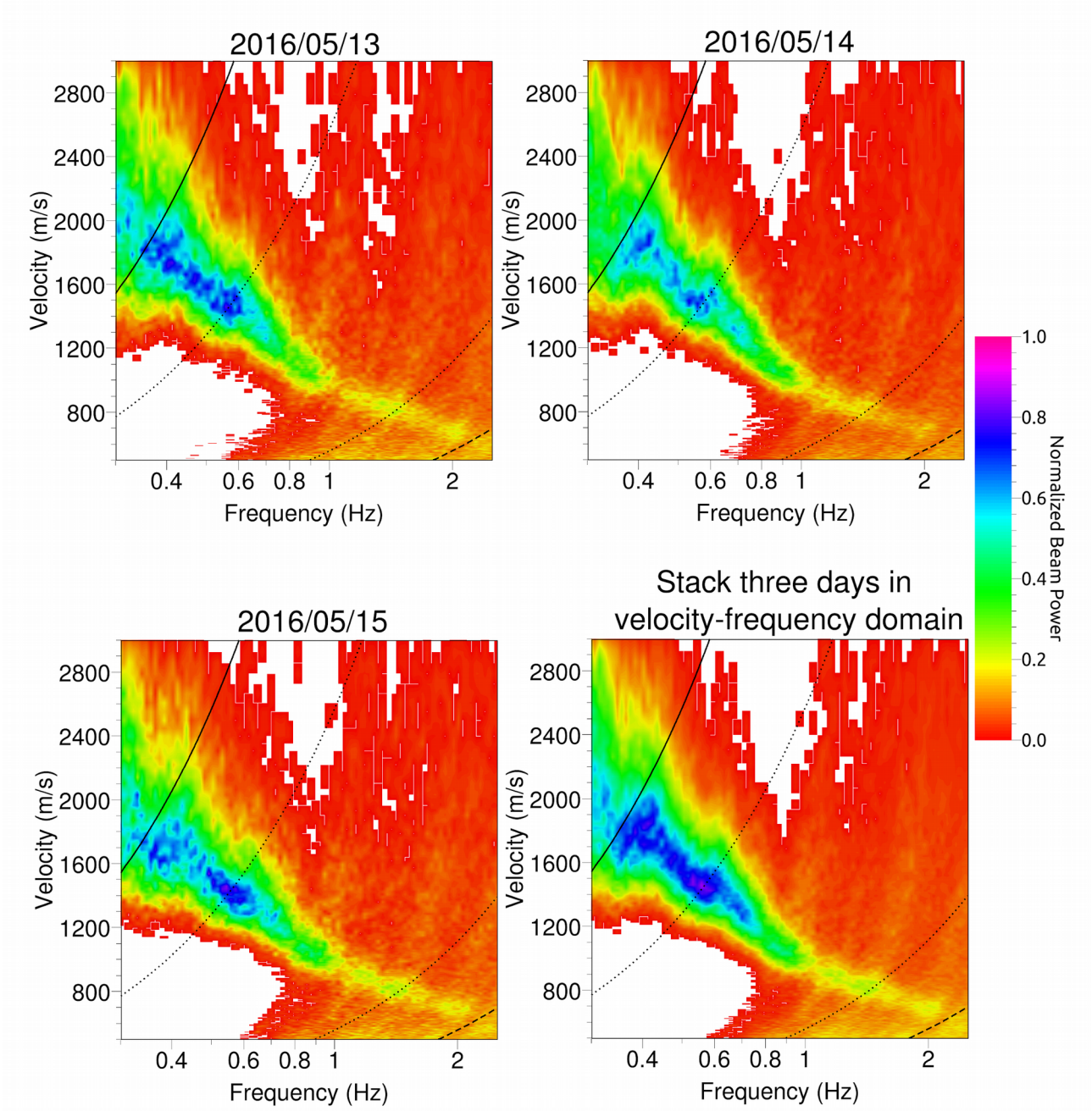

Figure S4: Results of fk analysis on data acquired by temporary seismic network in three different days and stack of different results. The acquisition day and the stack are reported on the top of respective panels. The colour scale is proportional to the beam power and the resolution and alias limits of the array are shown as thin black curves.

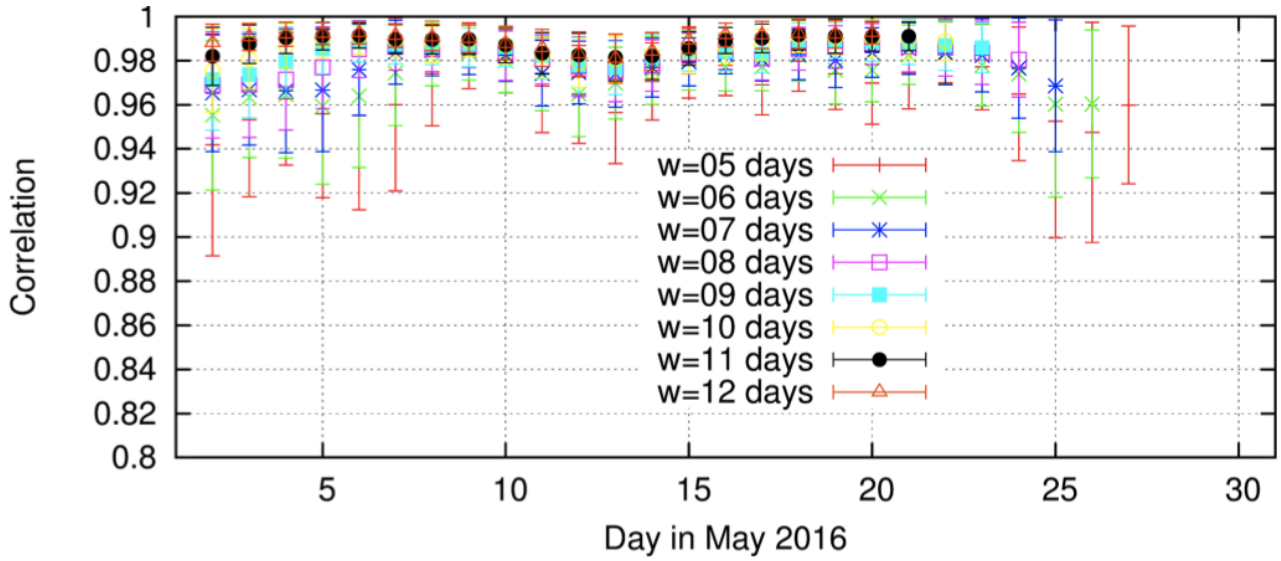

Figure S5: Results between the comparison of the stacks computed add all the daily CCs (SCCm) over the entire acquisition duration (1 month) and in mobile windows of different durations (SCCw) between 5 and 12 days. The dots and lines represent the means and standard deviations of maximum of cross-correlation computed between SCCm and SCCw for the different station pairs. The values are calculated for the different window lengths and for the different starting times.

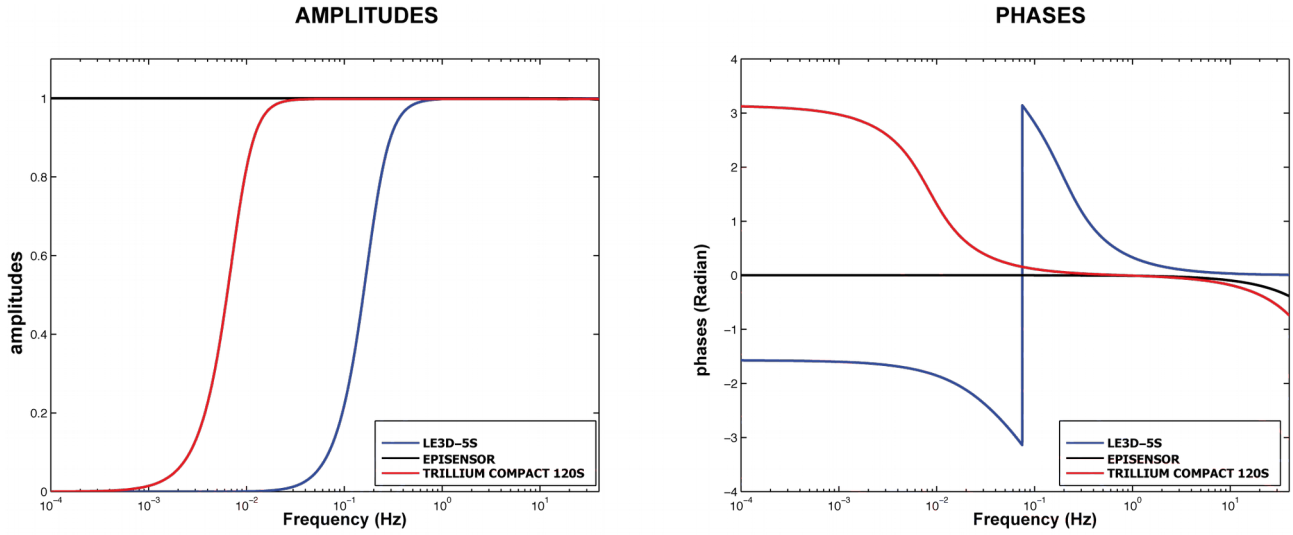

LE3D-5S

Normalizing factor: 1
Sensitivity: 400 V/ms^{-1}

ZEROS (rad/s):	POLES (rad/s):
0	-0.888000 +0.888000 j
0	-0.888000 -0.888000 j
0	-0.290000

EPISENSOR

Normalizing factor: 2.46E+13
Sensitivity:2.0387 V/ms^{-2}

POLES (rad/s)
-9.810000E+02 -1.009000E+03 j
-9.810000E+02 +1.009000E+03 j
-3.290000E+03 -1.263000E+03 j
-3.290000E+03 +1.263000E+03 j

TRILLIUM COMPACT 120

Normalizing factor: 8.18400E+11
Sensitivity 750 V/ms^{-1}

ZEROS (rad/s):	POLES (rad/s)
0	-3.691000E-02 -3.712000E-02 j
0	-3.691000E-02 +3.712000E-02 j
-434	-3.712000E+02
	-3.739000E+02 -4.755000E+02 j
	-3.739000E+02 +4.755000E+02 j
	-5.884000E+02 -1.508000E+03 j
	-5.884000E+02 +1.508000E+03 j

Figure S6: Instrumental response of the three types of sensors used in the study: at the top of figure the amplitudes and the phases response are displayed at the bottom a table including all parameters characterizing seismic sensors (poles and zeros, normalizing factor and sensitivity).